A simplified design procedure for seismic upgrade of frame structures equipped with hysteretic dampers

Authors

Eleonora Bruschi[(a)]; Virginio Quaglini[(a)]; Paolo M. Calvi[(b)]

Affiliation:

[(a)] Politecnico di Milano, Department of Architecture, Built Environment and Construction Engineering, Piazza Leonardo da Vinci 32, 20133 Milan, Italy;

[(b)] University of Washington, More Hall, Department of Civil and Environmental Engineering, Seattle, WA 98195, USA;

e-mail address:

eleonora.bruschi@polimi.it ; pmc85@uw.edu ; virginio.quaglini@polimi.it

Corresponding Author

Virginio Quaglini, MSc, PhD

Politecnico di Milano, Department of Architecture, Built Environment and Construction Engineering, Piazza Leonardo da Vinci 32, 20133 Milan, Italy

e-mail: virginio.quaglini@polimi.it

Abstract

This paper presents a simple and affordable design procedure for the seismic upgrade of frame structures equipped with hysteretic dampers. The proposed framework is aimed at leading the designer to proportion the damper device(s)) in order to achieve a desired structural performance level. According to the method, the structural system composed by frame and dampers is replaced by an equivalent Single Degree of Freedom (SDOF) system, characterized through its secant stiffness and equivalent viscous damping, both defined in relation to a "performance point" which is assigned on the basis of the allowable damage of the frame and on the first mode deformation of the main structure. The global stiffness and strength of the equivalent SDOF system are then distributed along the height of the frame according to a stiffness-proportionality criterion, and the properties of the damper units are calculated depending on the chosen layout. Two case-studies relevant to as many reinforced concrete frames are provided to demonstrate the effectiveness of the suggested procedure, obtaining a satisfactory agreement between the design target and numerical capacity curves. Non-linear dynamic analyses are further performed to assess the reliability of the methodology.

Keywords

Design procedure; Frame structures; Damper brace; Hysteretic damper; Capacity Spectrum; Seismic retrofit; Non-linear analyses.

1. Introduction

Supplemental energy dissipation in structures is typically achieved by incorporating energy dissipation devices, commonly referred to as dampers, intended to absorb much of the earthquake input energy thus eliminating or limiting the damage to the structural frame. It is noteworthy that, if necessary, energy dissipation devices can be easily replaced at the end of the seismic event [1]. Current dampers can be classified in two categories [1]: (i) viscous dampers, which provide dissipation through the lamination of a viscous fluid forced to pass through an orifice or a valving system, and whose behavior mainly depends on the velocity; and (ii) hysteretic dampers, whose behavior mainly depends on the imposed displacement, and which are further classified into hysteretic steel dampers, friction dampers and metal extrusion dampers, depending on the energy dissipation mechanism.

A common practice for the seismic upgrade of existing structures using supplementary energy dissipation systems consists in determining the size and the suitable location of the dissipation units within the building starting from a trial configuration based on the engineer's expertise and assessing the retrofitted structure through dynamic or static analyses [2]. The properties and/or the number of the added dissipation units are iteratively changed until the target performance is reached. It is evident that this trial-and-error approach can be a laborious task.

Several procedures have been proposed in recent years for the design of supplementary energy dissipation systems and some of them are based on the Direct Displacement-Based Design (DDBD) method [3]. In the DDBD approach [4], a target displacement demand is defined and related to a given inter-story drift that a structure should achieve when subjected to the design earthquake. Based on the target displaced configuration, a "substitute" SDOF model is defined and used to replace the multi-degree of freedom (MDOF) structure. The substitute SDOF model consists of an equivalent linear system, characterized by an effective (secant) stiffness and an effective energy dissipated, represented through an equivalent damping ratio. The design displacement of the equivalent SDOF structure is used in combination with the design displacement response spectrum, to determine the

effective period of the substitute structure and, in turn, its effective stiffness. The design base shear is then obtained as the product of the design displacement of the SDOF system and its secant stiffness [5]. Over the years, this approach has been implemented to design new structures and efforts have been made by several authors to adapt the DDBD method to the design and retrofit of structures equipped with dissipating devices [5]-[12], by incorporating an equivalent viscous damping term proportional to the energy dissipation provided by the dampers [3]. It is also worth mentioning the procedure described by Levy et al. [13] who use an equivalent SDOF system to obtain the optimal period of the braced structure by performing a full non-linear dynamic analysis for a set of recorded ground motions.

Kim and Choi [2] applied the general procedure of the DDBD documented in the SEAOC Blue Book [14] in reverse order for evaluating the seismic performance of an existing structure. In principle the procedure is similar to the Capacity Spectrum Method [15], in that the design performance point is determined as the point where the displacement demand of the earthquake equals the plastic deformation capacity of the structure. However, the displacement response spectrum instead of the acceleration-displacement response spectrum (ADRS) is used, and the required damping is calculated as the difference between the total effective damping needed to meet the target displacement and the equivalent damping provided by the structure at the target displacement. For viscous dampers the design process ends here, while for dampers with stiffness, such as viscoelastic or hysteretic dampers, iterations are required because the introduction of the devices increases the stiffness of the system as well. In that case, the capacity curve of the structure needs to be redrawn considering added dampers, and the process is repeated until convergence.

Mazza and Vulcano [16]-[18] developed a building retrofit procedure according to the Performance-Based Design in order to achieve, for a given seismic intensity level, a specified performance objective, for example an assigned level of damage of either the structural or non-structural elements. The procedure aims at controlling the inter-story drifts of the building and, in particular, a

proportional stiffness criterion, which assumes the elastic lateral story-stiffness due to the dissipating braces (K_{DB}) proportional to that of the unbraced frame (K_F), is combined with the DDBD method, in which the design starts from the target deformation. In this iterative approach, the ratio K_{DB}/K_F is assigned depending on the strength of the unbraced frame and on the protection level expected for the building, and is kept constant at each story throughout the whole procedure. Though initially conceived for essentially regular structures, it has been extended to in-elevation irregular framed structures ([19], [20]) and unsymmetric-plan structures ([21], [22]).

Lin at al. [23] adapted their original method, initially formulated for the design of new and regular buildings equipped with generic energy dissipation systems [6], to retrofit existing buildings using non-linear viscous dampers based on the concept of equivalent linear system. In this method, the location and properties of the dampers need to be established at the beginning of the process. Londono et al. [24] provided an additional tool, complementary to conventional damper design strategies, that can be used to calculate the stiffness required by the supporting brace to provide the specified effectiveness of the damping action. Raju and Iyer [25] developed a methodology useful for finding the capacity and the distribution of viscous fluid dampers fitted in different mechanisms (specifically in chevron, upper toggle and scissor jack mechanisms) located in buildings.

Bergami and Nuti [26] developed a general procedure, valid for any typology of dissipative brace, intended to achieve the following performance objectives: (i) protect the structure against structural damage or collapse; (ii) avoid non-structural damage; and (iii) avoid excessive base shear. This DDBD approach is based on the Capacity Spectrum Method [27] and consists of an iterative procedure where the capacity curve of the braced structure is evaluated at each iteration step considering the different contributions of the as-built structural frame and of the damped brace systems. The desired performance of the structure is selected as the target displacement corresponding to a selected limit state for a given seismic action, and the additional damping introduced from the

dissipative brace system is estimated as the difference between the total damping required to achieve the performance point, and the hysteretic damping of the structure without braces.

Di Cesare and Ponzo [28] focused on steel hysteretic brace systems and proposed an iterative procedure intended to control the maximum inter-story drifts, by regularizing the stiffness and strength along the height of the braced building according to the regularity criteria provided by seismic codes (e.g. [29], [30]). This method has found applications in some recent publications ([31], [32]).

Barbagallo et al. [33] focused on the retrofit of existing reinforced concrete (RC) frame buildings using Buckling Restrained Braces (BRBs). The authors highlighted that all the procedures in the literature do not allow a direct control of drift demand; for this reason, they proposed an iterative method, consistent with the prescriptions of Eurocode 8 (EC8) [29], to determine the size of BRBs at each story. Differently from the previous methods, this approach operates on the MDOF system (not on the substitute SDOF) and the non-linear static analysis is performed only to evaluate the internal force of the frame members.

Ferraioli and Lavino [3] identified some critical aspects common to all the previous methods: (i) the frame-damped brace interaction is neglected, as no method considers the increase of the axial force in the frame columns and the consequent reduction of the deformation capacity; (ii) the proportional stiffness criterion commonly adopted to distribute the damper properties along the height of the frame may produce a non-uniform distribution of peak story drift under earthquake ground motions, not preventing soft-story mechanisms. Moreover, the existing methods generally include only the first mode contribution, neglecting the influence of higher modes in the response of MDOF elastoplastic systems, and in case of asymmetric-plan buildings the behavior of the RC bare frame is dominated by the torsional effects, which disappear when the damped braced structure is analyzed. For this reason, the authors divided their procedure in two phases: in the first phase, a preliminary design of the dissipative braces is conducted, and relevant properties and position are determined according to

the method of Mazza and Vulcano [18]; in the second phase, the Displacement-based Adaptive Pushover (DAP) [34] is carried out and an adaptive version of the Capacity Spectrum Method is developed (starting from the classical version of Fajfar [27]), in order to overcome the assumptions that the structure vibrates predominantly in a single mode and that the dynamic properties of the structure remain unchanged after the insertion of the braces.

Recently, Nuzzo et al. [35], [36] proposed a procedure, similar to the one of Bergami and Nuti [26], valid for design and retrofit of frame structures equipped with hysteretic dampers, taking into account the flexibility of the supporting brace, usually provided to connect the device to the external frame. However, differently from reference [26], the pushover analysis is performed only at the beginning of the procedure in order to define the capacity curve of the bare frame, while in the following steps, the capacity curve of the braced frame is evaluated by means of simple analytical equations.

Some authors proposed simplified procedures to directly determine the characteristics of the supplementary energy dissipation systems avoiding iterations. Diotallevi et al. [37] focused on non-linear viscous dampers and based the retrofit procedure on a new dimensionless parameter, called damper index, which has been introduced in the equations of motion. This method was later extended by Landi et al. [38] to include the case of structures exceeding the elastic limit.

Other authors decided to adopt energy-based methods. Silvestri et al. [39] and Palermo et al. [40] proposed a 5-steps energy-based procedure for the dimensioning of viscous dampers, starting from the practical indications given by Christopoulos and Filiatrault [1]. The method is direct, no iterations are needed, and it does not require to introduce fictitious springs, since only the additional damping is considered; differently from the other procedures, this method requires the application of time history analyses instead of pushover analyses.

Durucan and Dicleli [41] proposed an iterative energy-based approach to upgrade the performance of seismically vulnerable RC buildings. The methodology is based on the equal energy dissipation principle, whereby the energy dissipated by an elastic system can be assumed to be equal to that

dissipated by an identical (non-linear) system that yields at a certain lateral force level. The difference between the areas under the elastic and inelastic base shear force vs. roof displacement curves is the required additional energy that needs to be absorbed by the retrofitting system.

Terenzi [42] improved the method originally proposed [43], focusing on the retrofit of RC structures upgraded with fluid viscous dampers. This approach does not require any preliminary evaluation of the input energy demand and is intended only for relatively stiff frame structures, where the seismic performance can be enhanced by incorporating a supplementary damping system with limited stiffness capacity.

Finally, De Domenico et al. [44] presented a deep review of different design strategies for the protection of buildings using fluid viscous dampers, concluding that energy-based design strategies provide the best method to define the optimal damper distribution in the building, and permits a global control of the seismic response including displacements, accelerations, forces and energy-specific quantities.

As a matter of fact, most of the methods presented above are not straightforward and nowadays many practitioners still have little confidence in supplementary energy dissipation strategies, especially for applications to ordinary constructions where simple and affordable methods may foster the adoption of seismic mitigation strategies based on damper technology. The present study proposes an effective and easy to use procedure for the seismic upgrade of existing frame structures by means of hysteretic damped braces. The procedure is suitable for professional applications and consists of two main parts: (i) a simple method to define the global properties of the damped brace system, described by means of an equivalent SDOF system; and (ii) a strategy to determine the distribution of the properties of the equivalent SDOF damped brace along the height and across each floor of the structure.

The procedure to calculate the global properties of the energy dissipation system is based on the Capacity Spectrum Method [15][27]. Similarly to the method [35], the capacity curve of the main frame is determined at the beginning of the process via non-linear static analysis (NLSA), while the

capacity curve of the braced frame is defined by simple analytical equations, thus providing an iterative procedure that converges in few steps and that can be implemented in a spreadsheet.

The second part of the procedure is focused on distributing the effective properties of the damped brace system along the height and across the stories of the building. A method, derived from the literature and based on the principle of distributing the stiffness and strength proportionally to the stiffness of each floor calculated via dynamic analysis is presented. Finally, the properties of the dissipation braces at each floor are determined accounting for the actual number and layout of the devices.

The ease and effectiveness of the method is illustrated analyzing two RC buildings. The first structure is an existing 4-story frame building located in a medium/high seismic area and designed according to outdated standards [28], which needs to be retrofitted to comply with the performance requirements of the most recent Italian norm [30]. The second structure is a residential 6-story building, designed according to the current Italian Building Code [30] for a low seismicity zone [45], which is upgraded to resist higher seismic excitations corresponding to a high seismicity area. Both structures are supposed to fail in flexure and specific issues, typical of existing buildings (namely, shear failure of beams, columns, or beam-column joints) are not taken into account in the numerical models.

The procedure is applied to the two case-studies and illustrated step by step, discussing the main results. The effects of the distribution of the damper properties at the various floors are also highlighted by examining, as an alternative to the method recommended in the procedure, a second procedure available in the literature. Non-linear static and dynamic analyses (NLSA and NLDA) are eventually performed.

It must be finally mentioned that, though the case-studies presented in the paper refer to RC structures, the procedure herein proposed has been formulated for conventional, flexible framed structures and is applicable to steel structures as well.

2. Design Procedure of the Damped brace System

This section presents a design methodology for the upgrade of an existing structure via hysteretic dampers, to achieve the specified performance level. The design procedure is based on the Capacity Spectrum Method [46]: the required performance is expressed in terms of a target displacement demand, associated to the acceptable damage to the main frame, and the structural response is obtained by reducing the demand response spectrum as a function of the additional damping introduced by the supplementary energy dissipation. Iterations are required since the addition of braces increases the stiffness of the system and the capacity curve has to be continuously updated as the characteristics of the damped braces are defined.

The procedure is applicable to frame buildings equipped with hysteretic dampers with behavior dependent solely on the axial deformation, and insensitive to velocity. The non-linear response of the bare structure is initially estimated by performing a pushover analysis on the multi-degree of freedom (MDOF) frame and then idealized as the bilinear curve of an equivalent single-degree of freedom (SDOF) system, as prescribed in Eurocode 8 – Part 1 [47]. The equivalent SDOF unbraced frame (F) and the damped brace (DB) systems are considered as bi-linear springs working in parallel, providing the equivalent response of the combined Frame + Damped Brace (F+DB) system, Figure *1*.

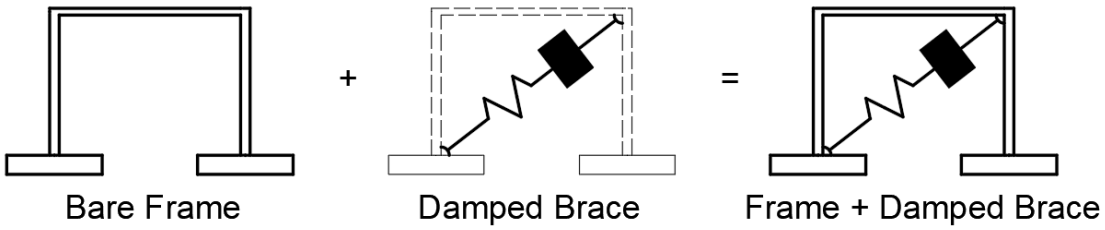

Figure 1: Rheological model of the unbraced frame, the damped brace and the combined braced frame systems

The theoretical force–deflection curve of a hysteretic damper is shown in Figure *2*, where N_D is the output force, d_D is the axial deflection, N_{yD} and d_{yD} are the yield force and yield deflection of the

device, N_{uD} and d_{uD} are the ultimate force and deflection, and $r \geq 0$ is the hardening parameter; the area enclosed in the hysteresis loop corresponds to the energy dissipated by the damper during a cycle. $K_D = N_{yD}/d_{yD}$ is the initial or elastic stiffness and $K_{2,D} = r\,K_D$ is the post-yield stiffness. Hysteretic dampers can have either a hardening behavior with positive post-yield stiffness ($r > 0$), or an elastic-perfectly plastic behavior ($r = 0$), which provides an output force independent on the accommodated deflection [48]. In the description of the procedure, hysteretic dampers with elastic-perfectly plastic behavior are assumed, but the method can be generalized to dampers with any $r \geq 0$.

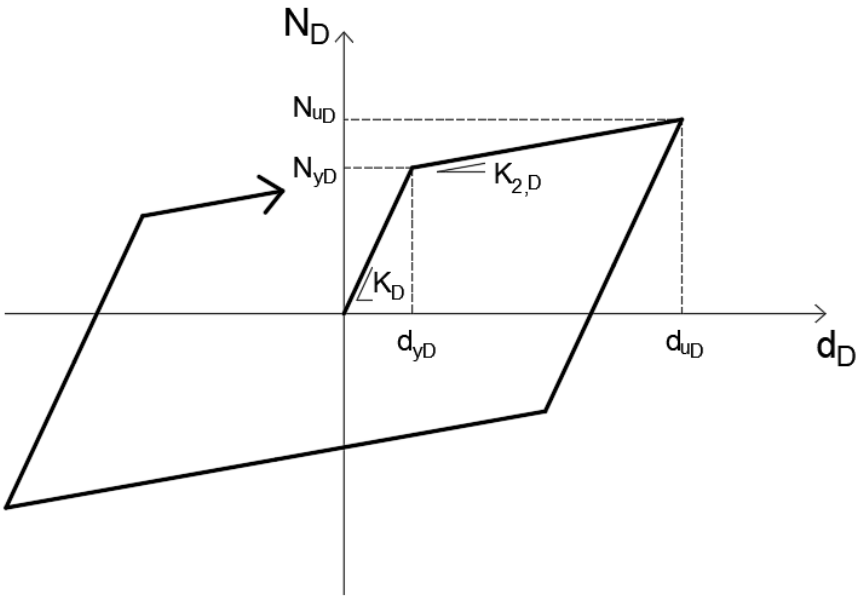

Figure 2: Theoretical force – deflection diagram of hysteretic dampers

The method is developed in the acceleration-displacement response spectrum (ADRS) space and the DB capacity curve is obtained as the difference between the capacity curve of the F+DB system achieving the target displacement, and the capacity curve of the main frame F. Then, the mechanical properties of the identified equivalent SDOF damped brace are distributed at each story according to a proportionality criterion with respect to the first mode properties of the unbraced frame.

The design procedure, which consists of 5 steps, is schematically shown in the flowchart in Figure *3* and detailed through the following sub-sections, each one corresponding to a single step of the framework. It is necessary to recall that a pre-requisite for the application of the procedure is that the behavior of the frame building is governed by the first mode, which legitimates the condensation of the MDOF structure to the equivalent SDOF system.

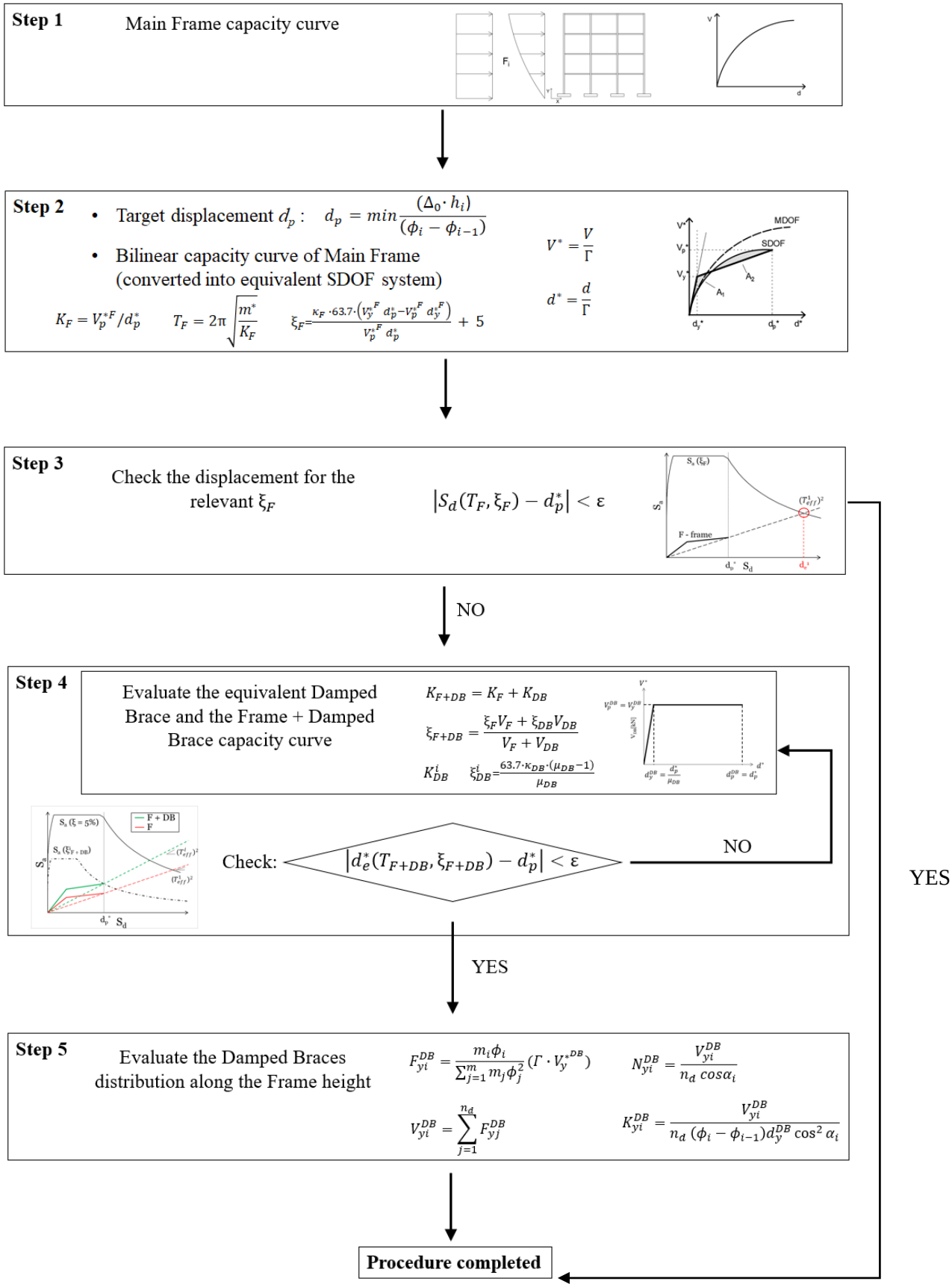

Figure 3: Flowchart of the proposed procedure

2.1 Define the capacity curve of the Main Frame

In the first step of the procedure, the capacity curve of the as-built structure is evaluated via a non-linear static analysis: the structural frame is statically loaded with gravity loads combined with a set of lateral forces to calculate the relationship between the lateral force and the lateral displacement of a suitable point of the structure, e.g., the center of mass of the roof. According to the prescriptions of [47], two lateral load distributions are considered: a uniform pattern, proportional to the floor masses m_i (with $i = 1 \div n$, where n is the total number of floors) and a modal pattern, obtained multiplying the first mode eigenvector components ϕ_i by the corresponding floor masses m_i. The load distributions are applied in both the positive and negative direction of each axis, considering 5% accidental eccentricity of the center of mass of each story [47]. For each load distribution the relevant base shear force vs. roof displacement ($V_F - d_F$) curve is calculated, and the lowest curve is taken as the capacity curve of the main (unbraced) structure.

The $V_F - d_F$ capacity curve of the MDOF structure is then converted to the $V_F^* - d_F^*$ capacity curve of the equivalent SDOF system through the modal participation factor Γ (Eq. 1) [27], [47]. The displacement d_F^*, the force V_F^* and the mass m^* of the equivalent SDOF system are determined via equations (2) – (4):

$$\Gamma = \frac{\sum_{i=1}^{n} m_i \phi_i}{\sum_{i=1}^{n} m_i \phi_i^2} \quad (1)$$

$$d_F^* = \frac{d_F}{\Gamma} \quad (2)$$

$$V_F^* = \frac{V_F}{\Gamma} \quad (3)$$

$$m^* = \sum_{i=1}^{n} m_i \phi_i \quad (4)$$

2.2 Identify the target displacement and define the equivalent bilinear capacity curve of the Main Frame

The target displacement d_p of the structure is identified depending on the required level of performance in accordance with the assumed design code. By referring to, e.g., the Italian Building Code (IBC) [30], the target displacement d_p can be chosen in order to fulfill the limits recommended in Table 7.3.III of IBC for the protection of both structural and non-structural elements. For example, depending on the considered limit state, the target displacement limiting damage to non-structural elements corresponds to a maximum inter-story drift ratio Δ_d ranging between 0.5% and 0.75% [35].

In order to fit the required performance at each story, the lateral displacement at the top of the frame is bound to match the target displacement

$$d_p = min \frac{\Delta_d \cdot h_i}{\delta_i} \tag{5a}$$

where Δ_d is the target inter-story drift ratio, h_i is the height of the i^{th} story, and $\delta_i = (\phi_i - \phi_{i-1})$. The product $\Delta_d \cdot h_i$ represents the target drift of the i^{th} story, while δ_i is the difference between the first mode eigenvector components of the adjacent stories. If the inter-story height is uniform, i.e., $h_i = h_0$ for $i = 1, \ldots n$ (n = number of stories), then Equation (5a) can be simplified as

$$d_p = \frac{\Delta_d \cdot h_0}{\delta_{max}} \tag{5b}$$

with $\delta_{max} = max(\phi_i - \phi_{i-1})$.

By setting the ultimate displacement of the as-built structure equal to the identified target displacement $d_u = d_p$, the ductility of the main frame is defined as $\mu_F = d_p/d_y$ where d_y is the yield displacement of the frame. Obviously, if the target is that the structure remains in the elastic range, $\mu_F = 1$.

Once the target displacement d_p (and the corresponding base shear force of the main frame V_p^F) is assigned, the bilinear curve of the equivalent SDOF system is evaluated in accordance with reference

[26] and clause C.7.3.4.2 of reference [50]. Such equivalent bilinear curve is defined by three conditions, namely: (i) same initial stiffness as the initial stiffness of the MDOF capacity curve, (ii) crossing of the performance point (d_p^*, V_p^{*F}) where $d_p^* = d_p/\Gamma$ and $V_p^{*F} = V_p^F/\Gamma$, and (iii) equivalence of areas A1 and A2 between the two curves, as shown in Figure *4*.

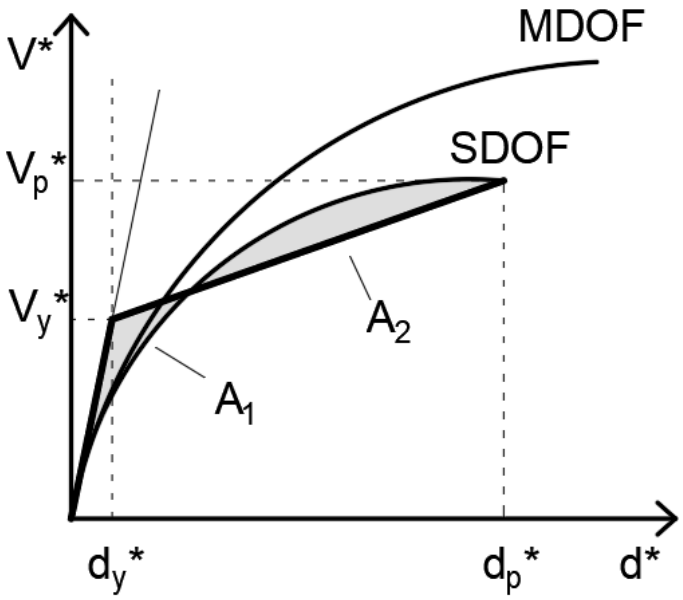

Figure 4: Definition of the equivalent bilinear curve according to [50]

Through the equivalent bilinear curve, the SDOF system is characterized by an equivalent secant stiffness $K_F^* = V_p^{*F}/d_p^*$ and an equivalent viscous damping ratio ξ_F (in percent) defined as in [49], [50]:

$$\xi_F = \frac{\kappa_F \cdot 63.7 \cdot \left(V_y^{*F}\, d_p^* - V_p^{*F}\, d_y^{*F}\right)}{V_p^{*F}\, d_p^*} + 5 \qquad (6)$$

where parameter κ_F accounts for the energy dissipation capacity of the bare structure and can be taken as 1.0 for structures with high damping capability (providing wide and stable hysteresis loops), 0.66 for structures with moderate damping capability (with moderate change of the hysteresis loops) and 0.33 for structures with low damping capability (with hysteresis loops affected by substantial pinching and decrease of area) [15]. On the right side of Eq. (6) the first term represents the

contribution of the inelastic deformation of the frame to the total equivalent damping, and the second term is the 5% inherent viscous damping of the structure. Though in the current literature the damping ratio to be considered in NLTH analyses of both RC and steel structures is estimated in the range of 0.5% to 2% [51]-[54], a 5% value is chosen in order to take into account the energy dissipation coming from possible infill panels or other non modelled non-structural components.

2.3 Check the displacement for the relevant ξ_F

The equivalent bilinear capacity curve $V_F^* - d_F^*$ is converted into the capacity spectrum in the acceleration-displacement response spectrum (ADRS) space, where the spectral coordinates are defined as $S_a = V^{*F}/m^*$ (acceleration in m/s^2) and $S_d = d_F^*$ (displacement in m).

The seismic action for the considered performance level is defined in terms of acceleration – displacement response spectra corresponding to different damping levels. For example, a 2% to 5% damped response spectrum is generally used to represent the demand when the structure responds as linearly-elastic, while higher damped response spectra are used to account for the hysteretic non-linear structural response of the system. To develop damped demand spectra, Equations (7.a) and (7.b) [47] are used in the procedure

$$S_a(T;\, \xi) = S_a(T;\, \xi = 5\%) \sqrt{\frac{10}{5 + \xi}} \qquad (7.a)$$

$$S_d(T;\, \xi) = S_d(T;\, \xi = 5\%) \sqrt{\frac{10}{5 + \xi}} \qquad (7.b)$$

where *T* is the period of vibration in seconds. Response spectra are generally plotted in S_a vs T or S_d vs T coordinates, however in order to have a direct comparison to the capacity spectrum, the response spectra are plotted in the acceleration-displacement plane, with a set of coordinates defined by S_a and S_d. It should be noted that when the spectral values are plotted in ADRS format, the period is represented by lines radiating from the origin [55].

The spectral displacement of the main frame for the considered seismic action is determined analytically. The secant stiffness of the capacity spectrum to the target displacement $K_F^* = {V_p^*}^F / d_p^*$ is used to calculate the effective period of the main structure $T_F^* = 2\pi\sqrt{\frac{m^*}{K_F^*}}$ and hence the corresponding spectral displacement $S_d(T_F^*;\, \xi_F) = S_d(T_F^*;\, \xi = 5\%)\sqrt{\frac{10}{5+\xi_F}}$ where ξ_F is the equivalent viscous damping ratio of the unbraced structure defined by Eq. (6). If $S_d(T_F^*;\, \xi_F) \leq d_P^*$ the unbraced structure meets the performance requirement and the procedure ends (no retrofit is required). If $S_d(T_F^*;\, \xi_F) > d_P^*$ the main frame alone is unable to meet the performance level and the damped brace system must be introduced.

2.4 Evaluate the equivalent damped brace and the frame + damped brace capacity curve

An iterative procedure is used to evaluate the damped brace. In the first iteration the undamped structure is considered with effective stiffness $K_{eff}^1 = K_F^*$ and effective period $T_{eff}^1 = T_F^*$, with K_F^* and T_F^* defined above. The line radiating from the origin with slope $\left(T_{eff}^1\right)^2$ identifies, where it crosses the 5% damped response spectrum, the spectral displacement d_e^1 of an elastic oscillator with period T_{eff}^1 corresponding to the effective period of the unbraced frame at maximum response d_p^* , i.e. $d_e^1 = S_d(T_{eff}^1; \xi = 5\%)$ (Figure 5).

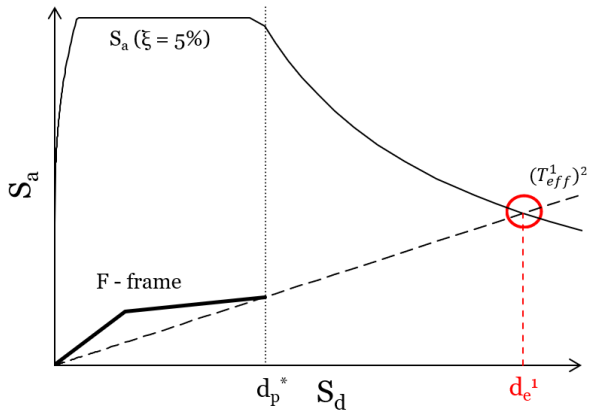

Figure 5: Evaluation of the spectral displacement d_e^1 at first iteration

In order to meet the target displacement d_p^*, additional damping must be supplied by the damped brace. According to Eq. (7.b), the total damping ξ_{eff}^1 required for the combined frame and damped brace (F+DB) system shall fulfill the displacement equality

$$S_d\left(T_{eff}^1;\, \xi_{eff}^1\right) = d_p^* \tag{8}$$

from which a first estimate of the effective viscous damping ξ_{eff}^1 is determined as

$$\xi_{eff}^1 = 10 \cdot \left(\frac{S_d\left(T_{eff}^1;\, \xi = 5\%\right)}{d_p^*}\right)^2 - 5 = 10 \cdot \left(\frac{d_e^1}{d_p^*}\right)^2 - 5 \tag{9}$$

The properties of the equivalent SDOF damped brace are determined as a function of ductility μ_{DB}, which is assigned as a design input depending on the employed damper technology. An optimal design ductility for hysteretic steel dampers is assumed in the range of $4 \div 10$ [31], whereas for friction and extrusion dampers there is no technological limitation to the displacement capacity that can be achieved without strength degradation [48]. The damper yield strength V_y^{DB}, which coincides with V_p^{DB} for devices characterized by an elastic-perfectly plastic behavior (Figure *2*), is instead the unknown of the procedure.

The equivalent viscous damping of the damped brace system ξ_{DB} is calculated according to expression [49]

$$\xi_{DB} = \frac{\kappa_{DB} \cdot 63.7 \cdot \left(V_y^{*DB}\, d_p^{*DB} - V_p^{*DB}\, d_y^{*DB}\right)}{V_p^{*DB}\, d_p^{*DB}} \tag{10}$$

and by setting the ultimate displacement of the equivalent SDOF damped brace equal to the target displacement $d_u^{*DB} = d_p^*$, which yields $d_y^{*DB} = d_p^*/\mu_{DB}$, Eq. (10) simplifies to Eq. (11):

$$\xi_{DB} = \frac{63.7 \cdot \kappa_{DB} \cdot (\mu_{DB} - 1)}{\mu_{DB}} \tag{11}$$

In Eqs. (10) and (11) the value of κ_{DB} can be selected based on experience and past applications or calibrated from experimental evidence.

The yield strength of the damped bracing system at first iteration $V_{y,1}^{*DB} = V_{p,1}^{*DB}$ is hence evaluated through the energetic equivalence of Eq. (12) [53]:

$$\xi_{eff}^{1} \cdot V_p^{*F} = \xi_F \cdot V_p^{*F} + \xi_{DB} \cdot V_{p,1}^{*DB} \tag{12}$$

where ξ_F is defined through Eq. (6). The introduction of the damped brace in parallel with the main frame yields an increase of $V_{p,1}^{*DB}$ of the total strength of the combined system F + DB at the target displacement d_p^*.

The bilinear curve of the equivalent SDOF model of the retrofitted structure is constructed and plotted in $S_a - S_d$ coordinates to check if the identified damped brace is appropriate. The ultimate displacement of the upgraded capacity curve is equal again to the target displacement d_p^*, while the correspondent base shear force is $V_{p,2}^{*F+DB} = V_p^{*F} + V_{p,1}^{*DB}$. The new equivalent SDOF *Frame + Damped brace* (F + DB) system is characterized by an equivalent viscous damping $\xi_{F+DB}^2 = \frac{\xi_F * V_p^{*F} + \xi_{DB} * V_{p,1}^{*DB}}{V_p^{*F} + V_{p,1}^{*DB}} + 5$ and by an effective stiffness and an effective period equal to $K_{eff}^2 = \frac{\frac{V_{p,2}^{*F+DB}}{m^*}}{d_p^*}$ and $T_{eff}^2 = 2\pi\sqrt{\frac{1}{K_{eff}^2}}$, respectively. The spectral displacement for the considered damping ratio is determined as $S_d\left(T_{eff}^2; \xi_{F+DB}^2\right)$ and checked against the target displacement d_p^*. If $\left|S_d\left(T_{eff}^2; \xi_{F+DB}^2\right) - d_p^*\right| / d_p^* \leq \varepsilon$ (with ε sufficiently small, e.g. 0.05), the process ends and the properties of the damped bracing systems at each floor are determined in the next step, otherwise the iteration continues until the difference between d_p^* and $S_d\left(T_{eff}^i; \xi_{F+DB}^i\right)$ (i = number of iteration) is sufficiently small, Figure *6*.

At the i^{th} iteration, the shear force at the target displacement d_p^* is updated as $V_{p,i}^{*F+DB} = V_p^{*F} + V_{p,(i-1)}^{*DB}$, and the equivalent viscous damping ratio of the equivalent SDOF *Frame + Damped brace* (F + DB) system is determined from Eq. (13):

$$\xi_{F+DB}^{i} = \frac{\xi_F \cdot V_p^{*F} + \xi_{DB} \cdot V_{p,(i-1)}^{*DB}}{V_p^{*F} + V_{p,(i-1)}^{*DB}} \quad (13)$$

The effective stiffness and the effective period are $K_{eff}^{i} = \frac{\frac{V_{p,i}^{*F+DB}}{m^*}}{d_p^*}$ and $T_{eff}^{i} = 2\pi\sqrt{\frac{1}{K_{eff}^{i}}}$, respectively. The required effective viscous damping at the i^{th} iteration is calculated according to Eq. (8) and is equal to $\xi_{eff}^{i} = 10 \cdot \left(\frac{d_e^i}{d_p^*}\right)^2 - 5$ (%), where $d_e^i = S_d(T_{eff}^{i}; \xi = 5\%)$. The strength of the equivalent SDOF damped brace is eventually calculated via Eq. (14), where the unknown quantity is $V_{p,i}^{*DB} = V_{y,i}^{*DB}$

$$\xi_{eff}^{i} \cdot \left(V_p^{*F} + V_{p,(i-1)}^{*DB}\right) = \xi_F \cdot V_p^{*F} + \xi_{DB} \cdot V_{p,i}^{*DB} \quad (14)$$

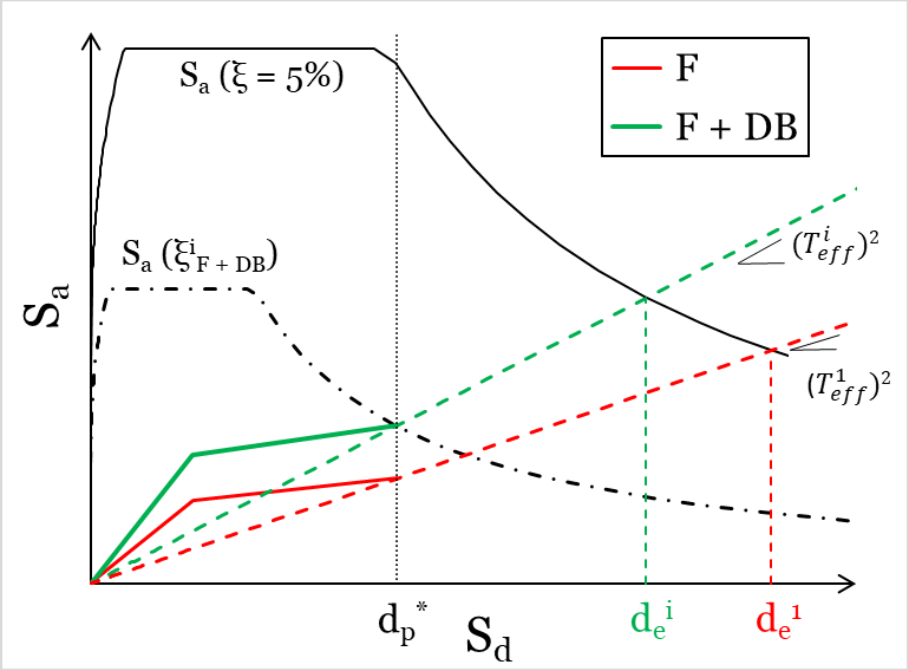

Figure 6: Graphical procedure for design of the damped braced structure

2.5 Evaluate the Damped Brace distribution along the Frame height

Once the properties of the equivalent SDOF damped brace are determined, their distribution across the stories of the structure is performed on the basis of a proportionality criterion ([16]-[22]).

The method uses, as input parameters, the yield properties (strength V_y^{DB} and displacement d_y^{DB}) of the equivalent SDOF damped brace and the components ϕ_i of the eigenvector associated to the first mode of vibration of the main frame. At each floor the properties of the braces equipped with hysteretic dampers are determined via Eq. (15) – (18), see Figure 7.

$$F_{yi}^{DB} = \frac{m_i \phi_i}{\sum_{j=1}^{m} m_j \phi_j^2} (\Gamma \cdot V_y^{*DB}) \tag{15}$$

$$V_{yi}^{DB} = \sum_{j=1}^{n} F_{yj}^{DB} \tag{16}$$

$$N_{yi}^{DB} = \frac{V_{yi}^{DB}}{n_d \, cos\alpha_i} \tag{17}$$

$$K_i^{DB} = \frac{V_{yi}^{DB}}{n_d \, (\phi_i - \phi_{i-1}) d_y^{DB} \cos^2 \alpha_i} \tag{18}$$

here N_{yi}^{DB} and K_i^{DB} represent the strength and stiffness of the single damped brace installed at the i^{th} floor, where n_d is the total number of dampers per floor chosen by the designer. At each floor, the damped braces are tuned in order to guarantee that the mode shape of the braced frame matches the first mode shape of the as-built structure [18], [19], [35]. If the frame remains elastic, the deformation remarks its fundamental mode shape, ensuring the same inter-story drift distribution [35]. It must be noted that Equations (17) and (18) which are used to calculate the properties of the individual damped brace refer to the diagonal configuration shown in Figure *7*, but can be easily modified to adapt to other configurations, such as chevron, upper toggle, etc.

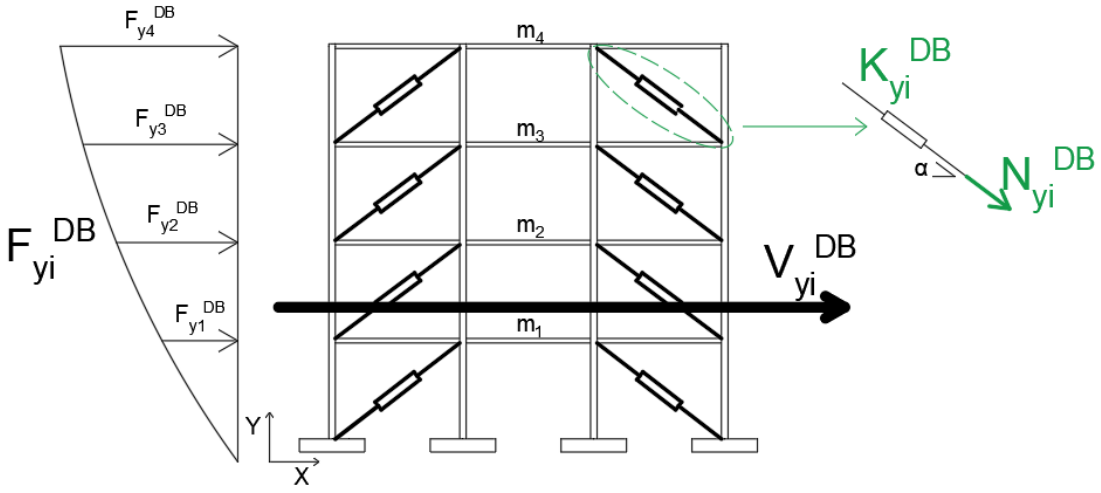

Figure 7: Quantities for design of diagonal braces with hysteretic dampers

It is worthnoting that the distribution method requires, as input variable, the number of damped braces at every story. This choice depends ultimately on the designer, who has to takle both architectural demands related to, e.g., the invasiveness of braces in facades, and economic issues related to local strengthening of columns and beams subjected to increase in internal forces due to the actions transmitted by the braces [57].

3. Application of the design procedure

The design method presented in Section 2 is applied to two case-study structures. The first structure is an existing 4-story reinforced concrete (RC) building located in Potenza (Italy) [28], a medium/high seismic area with PGA of 2.45 m/s^2, and it is assumed to be founded on soil type B with topographic factor T_1. The main dimensions of the building in plan and in elevation are sketched in Figure *8*; masses and additional information are reported in reference [28].

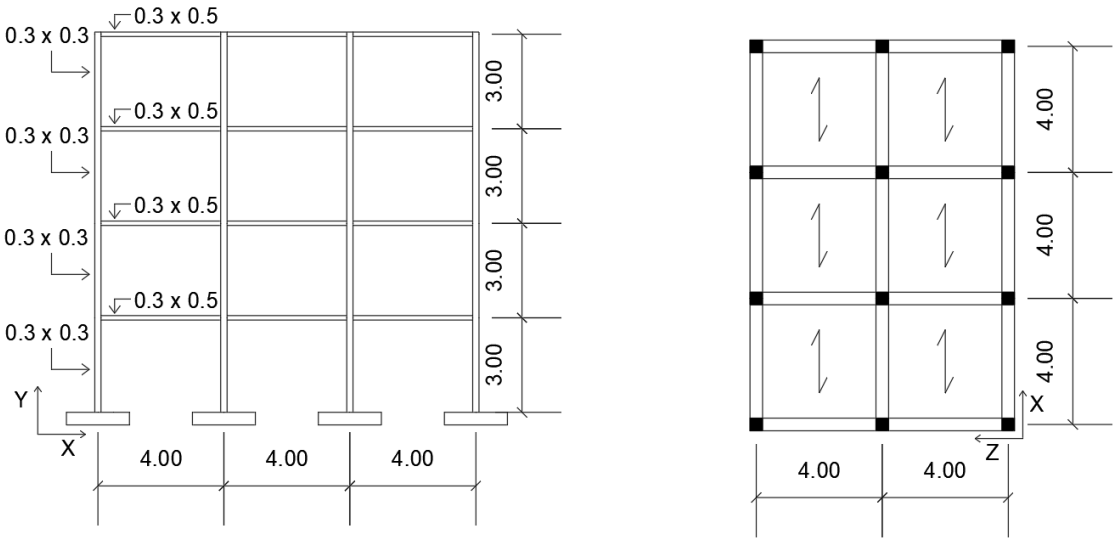

Figure 8: Existing RC frame building in Potenza: elevation and plan views

The second structure is a residential 6-story RC building, designed according to the novel Italian Building Code [30], which provides a similar approach to the Eurocode 8 [29], for a low seismicity zone corresponding to the municipality of Pordenone, Italy [45], characterized by a PGA = 1.91 m/s^2 and soil type B. This structure is upgraded to resist to higher seismic excitations corresponding to a high seismic area. Sketches of the building, with the main dimensions in plan and in elevation, are reported in Figure *9*; structural loads and additional design information are reported in reference [45].

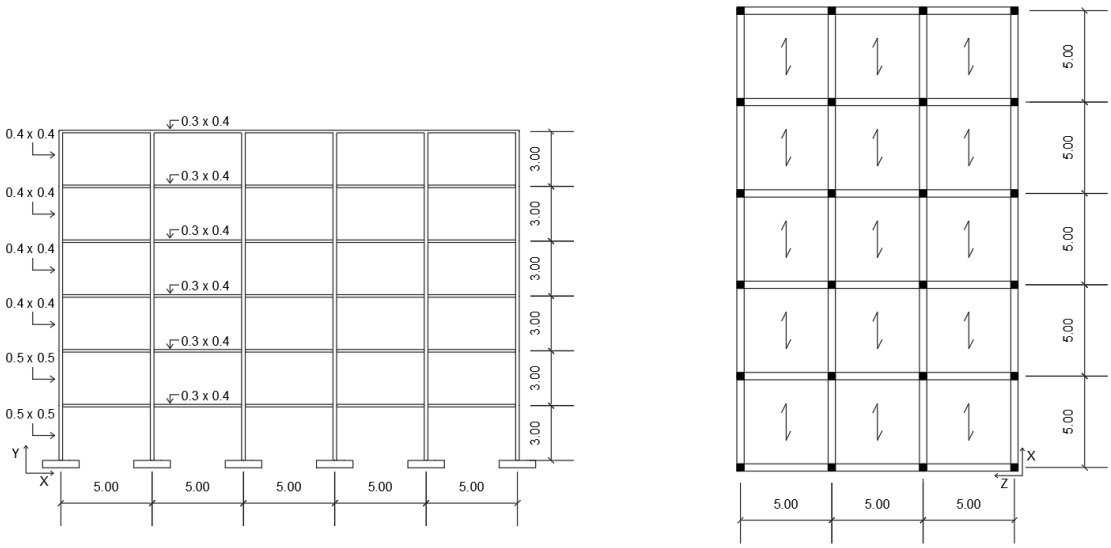

Figure 9: Existing RC framed building in Pordenone: elevation and plan views

Both structures are intended to fail in flexure, thus other failure mechanisms (such as shear failure of beams, columns or beam-column joints, bond slip and low-cycle fatigue, etc.) especially relevant to buildings designed according to outdated standards [56], are out of the scope of the present work.

For the seismic upgrade of both structures, steel braces equipped with hysteretic dampers characterized by an elastic-perfectly plastic behavior are used.

3.1 Numerical model of the RC case-study framed buildings

Full 3-D numerical models of both buildings are formulated within the OpenSees framework [58]. Beams and columns are modeled using the *forceBeamColumn* element object [59], in the form of the *beamWithHinges* element [60], assigning a linear elastic material behavior to the internal sub-element, whereas non-linearities can be activated only in the two external sub-elements. The length of the plastic hinge L_{pl} is evaluated with Eq.(19) in accordance with the Eurocode 8 [29], valid when a well-detailed confinement model of concrete is assumed [61]:

$$L_{pl} = \frac{z}{30} + 0.2h + 0.11\left(\frac{d_b f_y}{\sqrt{f_c}}\right) \quad (19)$$

In these plastic regions, the concrete non-linear behavior is modelled through a fiber section model, where each steel bar corresponds to a single fiber using uniaxial Giuffre-Menegotto-Pinto constitutive law [62], equivalent to *Steel02* material model with isotropic strain hardening [63]. The strain-hardening ratio b is assumed equal to 0.005 for the building in Pordenone, as specified in reference [45], and, in absence of any indication, equal to 0.01 for the building in Potenza [28], according to the modelling assumptions introduced in reference [61]. The parameters that control the transition from the elastic to the plastic branch are assigned as $R_0 = 18$, $C_{R1} = 0.925$ and C_{R2}= 0.15 [60]. The concrete model is implemented using the library uniaxial material *Concrete04*, which is based on the model proposed by Popovics [64]; the properties of the core region of the sections are evaluated referring to Equations (A6 – A8) of the Eurocode 8 [29] and the tensile strength of concrete is neglected in both core and cover regions [65]. It is worth mentioning that the material properties of the building are evaluated disregarding the confidence factors [29], [30]. In order to account for concrete cracking, the interior elastic sub-element is characterized by an effective area moment of inertia I_{eq}, equal to 50% of the gross area moment of inertia I_g, according to the provisions of the Italian and the European norms [47], [30].

The chosen modelling approach is consistent with the design code adopted [29], [47] and has been demonstrated to reproduce, with enough accuracy, the seismic response of RC members characterized by flexural behavior [61].

In all models, the masses of the structural members (beams, columns, and slabs) are concentrated at the master nodes, dead and live loads are uniformly distributed on each beam and have been calculated according to the tributary area concept; P-Delta effects are considered in the analysis, while bond slip and low-cycle fatigue effects are disregarded. The columns at the ground floor have fixed base supports, simulating rigid foundations. The damping of the frame is defined according to the

Rayleigh method, as a function of the tangent stiffness matrix only, assuming 5% viscous damping ratio, to take into account the energy dissipation coming from infill panels and other non modelled non-structural components [61].

The floor slabs are modelled as rigid diaphragms, by constraining the nodes belonging to the same floor to have the same displacement. An "axial buffer" [65] has been introduced in the FE model, through a *zeroLength* element object [66] characterized by a virtually zero axial stiffness and very high stiffnesses in shear and bending, placed between one end of each beam and the adjacent node belonging to the rigid diaphragm. This element works as an axial release to eliminate the fictitious axial force generated by the interaction between beam elements modelled with fiber sections and the rigid diaphragm [65].

The braces equipped with the hysteretic damper are modelled as truss elements [60] with an associated *uniaxialMaterial* model with elastic-perfectly plastic behavior [66].

3.2 Case-study 1: building in Potenza

The upgrade of the RC building in Potenza is carried out considering the seismic loads provided by IBC [30] for life-safety limit state (SLV), site of Potenza (Long 15° 48' 20.1744'', Lat 40° 38' 25.4688''), functional class cu = II, PGA = 2.45 m/s^2, soil type B and topographic factor T_1. Diagonal steel braces equipped with hysteretic dampers are inserted in the perimetral frames of each story, according to the layout shown in Figure 10.

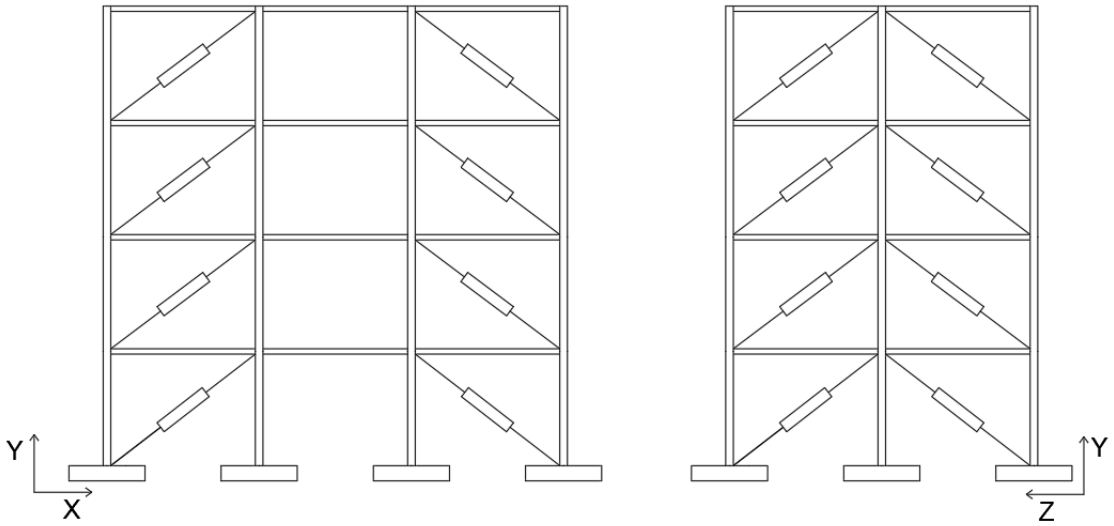

Figure 10: Layout of steel braces equipped with hysteretic dampers for case-study 1 building; the dissipative braces are installed in the perimetral frames

NLSAs are performed in both positive and negative directions of the two horizontal (X and Z) axes, applying horizontal force distributions proportional to either mass (referred hereinafter as UNIFORM) or modal (MODAL) properties, and considering 5% accidental eccentricity of the center of mass of each story, as prescribed in [30] and [47]. The MODAL capacity curve is the lowest in both directions (Figure 11) and is used to evaluate the main parameters of the equivalent SDOF systems, Eqs.(1) – (6) .

Since the building, designed in accordance with updated codes, is missing of seismic details, the hysteretic damper system is designed with the aim of keeping the main frame in the elastic range, limiting as much as possible structural damage. The target inter-story drift ratio is set to $\Delta_d =$ $0{,}005\ m/m$, corresponding through Eq. (5b) to the target displacement $d_p = 0.045\ m$ of the MDOF structure (h_0 = 3.0 m, $\delta_{i,max}$ = 0.3306), and d_p^* = 0.036 m of the equivalent SDOF system, respectively (Figure *11*). The equivalent bilinear capacity curves of the main frame in the two horizontal directions are then calculated according to Section 2.2 (Table 1). At the selected performance point the equivalent viscous damping ratio of the main frame is quite negligible (

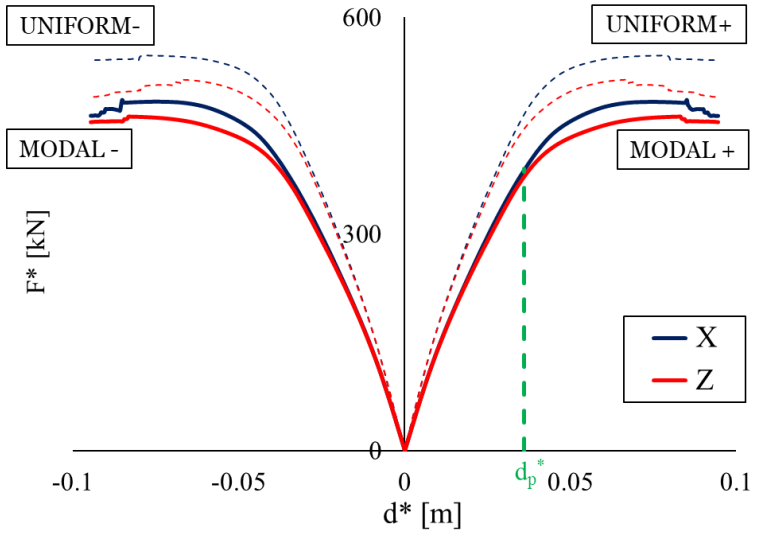

Figure 11: Determination of capacity curves in X- and Z- direction

Direction	Γ	d_y^*	V_y^{*F}	d_p^*	V_p^{*F}	ξ_F	m^*
	$[-]$	$[m]$	$[kN]$	$[m]$	$[kN]$	$[\%]$	$[ton]$
X	1.27	0.012	182	0.036	388	5.7	340
Z	1.27	0.012	186	0.0.036	385	6.4	339

Table 1: Properties of the equivalent SDOF system and bilinear capacity curves of case-1 structure in the two horizontal directions

The design procedure described in Section 2 is separately applied to both X and Z directions: the bilinear capacity curve of the equivalent SDOF model is represented in ADRS format (Figure 12) and the effective viscous damping ratio at first iteration ξ_{eff}^1 is determined by applying the Eq.(9).

The ductility of the equivalent damped brace system μ_{DB} is the design input. As the ductility factor for hysteretic steel dampers typically ranges between 4 and 10 [31], the upper and lower boundaries of the range, namely $\mu_{DB} = 4$ and $\mu_{DB} = 10$, are investigated. According to Eq.(11), the two ductility factors correspond to equivalent viscous damping ratios $\xi_{DB} = 47.8\%$ and $\xi_{DB} = 57.3\%$, respectively.

The bilinear curve of the equivalent SDOF *Frame + Damped brace* system in either horizontal direction is plotted in the ADRS plane to check if the identified damper is appropriate for the RC case-study frame (Figure 12). Step 4 of the procedure is iterated until the inelastic displacement of the equivalent SDOF braced structure converges to the target displacement d_p^* with $\varepsilon < 0.05$. As shown in Figure 13, convergence is always achieved within three iterations.

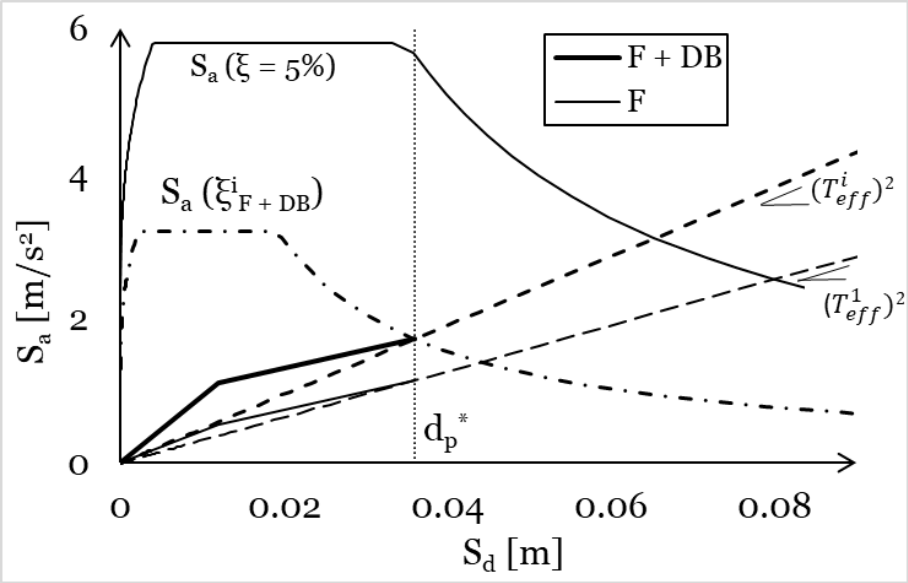

Figure 12: Equivalent capacity curves in X-direction of the main Frame (F) and Frame + Damped brace (F + DB) system with $\mu_{DB} = 10$ and relevant demand response spectra

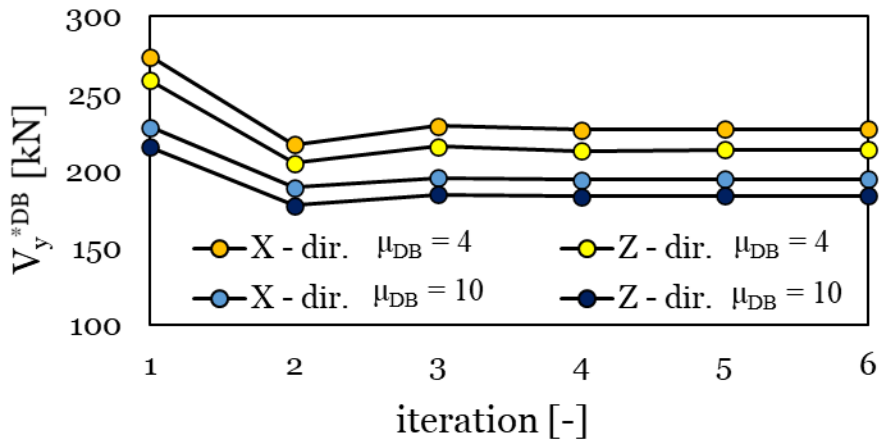

Figure 13: Iterative procedure for tuning the equivalent SDOF damped brace: damper yield strength vs. iteration number

The damped brace system is distributed along the height of the frame in accordance with the method illustrated in Section 2.5 (hereinafter called Method A). However, in order to highlight the effects of the damper distribution on the frame response, a second method described in literature ([28], [31] and [32]), named Method B, has been investigated as well.

By referring to the layout shown in Figure 10, with 4 dampers per story in each directions, the resulting strength and stiffness of the dissipating braces calculated with either method are reported in Table 2.

		$\mu_{DB} = 4$				$\mu_{DB} = 10$			
		Method A		*Method B*		*Method A*		*Method B*	
Directions	story	K_i^{DB} $[\frac{kN}{mm}]$	N_{yi}^{DB} $[kN]$	K_i^{DB} $[\frac{kN}{mm}]$	N_{yi}^{DB} $[kN]$	K_i^{DB} $[\frac{kN}{mm}]$	N_{yi}^{DB} $[kN]$	K_i^{DB} $[\frac{kN}{mm}]$	N_{yi}^{DB} $[kN]$
X	1st	31.5	90	29.2	54.6	67.4	77	62.5	46.7
	2nd	26.2	79	20.5	48.5	56.1	68	44	41.6
	3rd	26	56.7	19.3	36.2	55.5	48.6	41.4	31
	4th	24.4	26	17.7	19.2	52.3	22.3	38	16.5
Z	1st	29.1	84.7	26.5	51.5	62.6	73	57	44.3
	2nd	24	74.6	19	46	51.5	64.1	41	39.5
	3rd	23.6	53.5	18	34.2	51	46	38.5	29.4
	4th	22.12	24.5	16	18.2	47.6	21.1	34.3	15.6

Table 2: Case-study 1: properties of the damped braces for two assigned ductility factors

For both $\mu_{DB}s$, the recommended Method A provides the highest values of strength and stiffness of the damping braces. By considering, e.g., the X direction, the ratio between the stiffnesses determined according to either Method A or B varies from 1.08 at the first floor to about 1.40 at the fourth floor, and the ratio between the strengths varies from 1.65 at the first floor to 1.35 at the fourth floor. These figures do not change regardless of the damper ductility. Higher strengths are associated to $\mu_{DB} = 4$ than to $\mu_{DB} = 10$ in order to counteract the lower dissipation capacity.

Figure 14 compares in the ADRS plane the capacity curves of the upgraded building for $\mu_{DB} = 4$ (Figure 14 (a)) and $\mu_{DB} = 10$ (Figure 14 (b)); similar results are obtained along the Z-direction and not reported for conciseness.

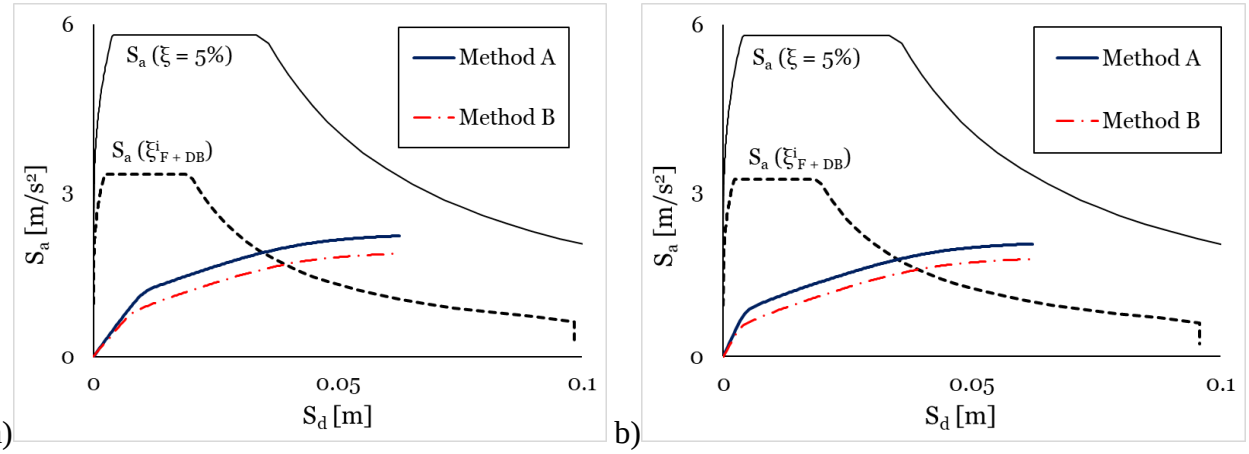

a) b)

Figure 14: Comparison of capacity curves in X-direction for different damped brace ductility: a) $\mu_{DB} = 4$; b) $\mu_{DB} = 10$

The design target is met by the upgraded frame for either value of μ_{DB}. However, regardless of μ_{DB}, the capacity curve of the structure upgraded according to Method A shows a stiffer response, and the performance point is characterized by a higher force at a smaller displacement, than its Method B counterpart.

NLSAs evaluate the response of the retrofitted structure in terms of global quantities only, such as the total base shear force and the displacement of the reference point, but do not provide any check on local quantities, like, e.g., drifts and forces at each story, and the damping capacity of the dissipating brace system inserted in the structure. To have a deeper insight, bidirectional non-linear dynamic analyses (BNLDAs) are performed in compliance with the IBC [30] and EC8 [47] considering two sets of seven artificial ground motions generated using the computer code SIMQKE [67]. The artificial accelerograms are characterized by a pseudo-stationary part of 10 sec and a total duration of 25 seconds as prescribed in [30], and are compatible on average with the elastic spectrum defined by the code [30] in the range of periods between 0.15 and 2 sec.

At the end of the BNLDAs, the response of the case-study structure has been evaluated considering engineering demand parameters such as absolute accelerations and inter-story drifts, which are commonly considered the main parameters to appraise the performance of frame structures and the effectiveness of the retrofitting technique. During the post-processing of the analysis, the mean value of the maxima of the parameters calculated for the seven pairs of bidirectional accelerograms has been evaluated for each direction. Figure 15-Figure 18 show the numerical results in terms of maximum inter-story drift ratio Δ and maximum Peak Floor Acceleration PFA at each story, comparing the as-built configuration to the retrofitted configurations with dissipating braces distributed according to either Method A or Method B, and considering either $\mu_{DB} = 4$ or $\mu_{DB} = 10$. The maximum values of Δ and PFA may not occur at the same time step of the analysis.

Figure 15 and Figure 17 show that inter-story drift ratios Δ drastically decrease when the damped braces are introduced. The damper distribution according to Method A produces at each floor, in either direction and for both values of μ_{DB}, maximum Δ values smaller than 0.5%, which is the design target drift ratio. In contrast, if Method B is adopted, Δ exceeds the specified limit at the second floor in the Z-direction for both $\mu_{DB}s$ (Δ = 0.0056 for $\mu_{DB} = 4$ and Δ = 0.0052 for $\mu_{DB} = 10$, Figure 15 and Figure 17). As expected [35], PFA increases in the braced structure (Figure 16 and Figure 18), and the increase is higher for the stiffer distribution following Method A: e.g., at the fourth floor PFA in X direction grows by either 12.6% with Method B or 28.4% with Method A, considering μ_{DB} = 4, while the increase is either 7.4% or 9.16%, respectively, with μ_{DB} = 10. The amplification of ground acceleration decreases by increasing the damping capacity of the dissipation system.

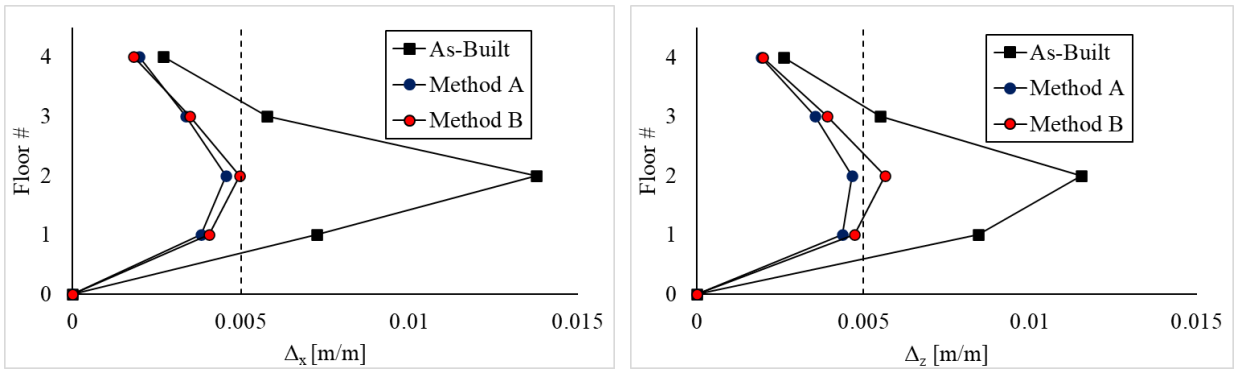

Figure 15: Comparison of maximum inter-story drift ratio Δ obtained by BNLDA with and w/o damped braces with $\mu_{DB} = 4$

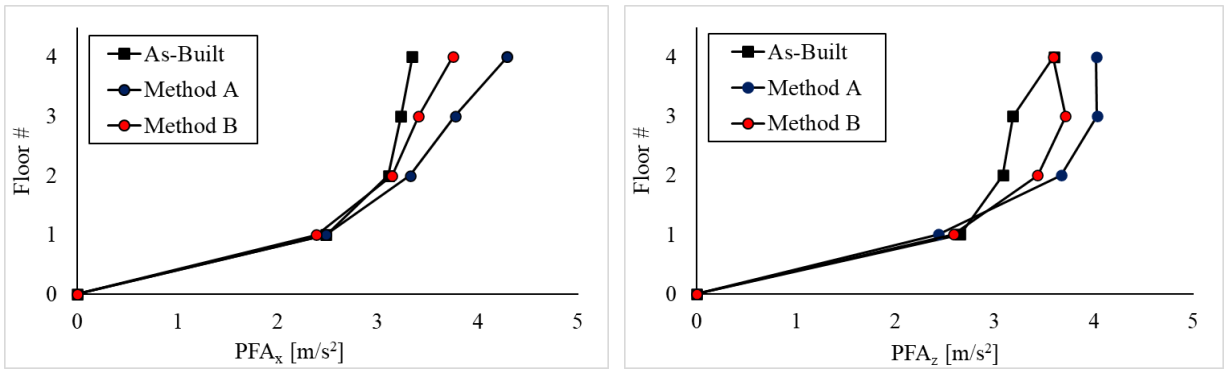

Figure 16: Comparison of maximum Peak Floor Acceleration PFA obtained by BNLDA with and w/o damped braces with $\mu_{DB} = 4$

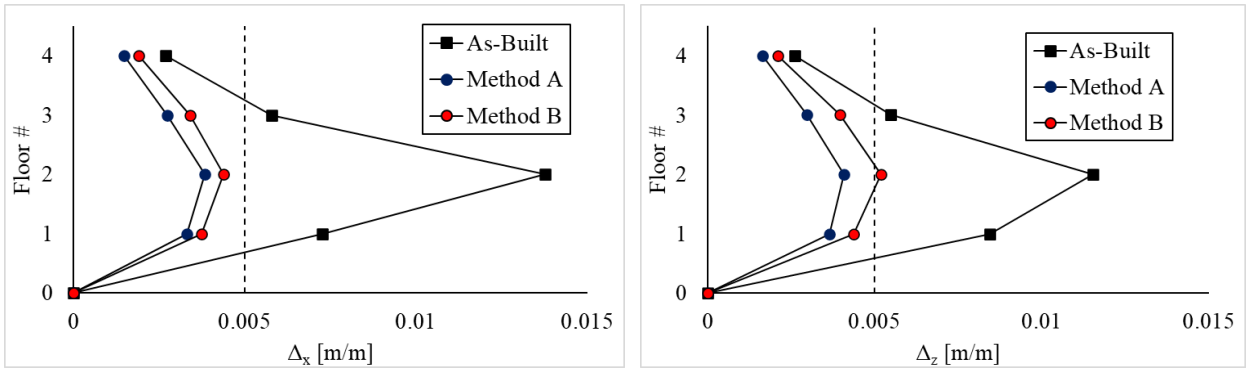

Figure 17: Comparison of maximum inter-story drift ratio Δ obtained by BNLDA with and w/o damped braces with $\mu_{DB} = 10$

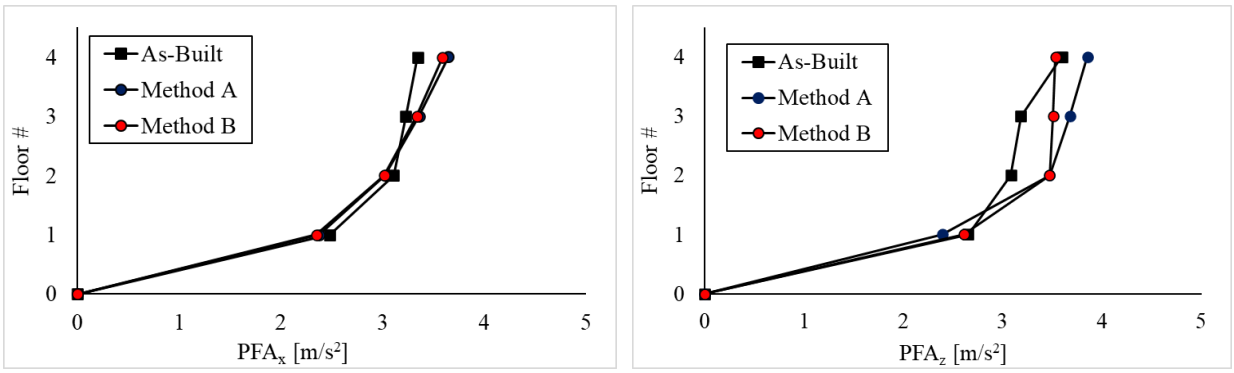

Figure 18: Comparison of maximum Peak Floor Acceleration PFA obtained by BNLDA with and w/o damped braces with $\mu_{DB} = 10$

Figure 19 and Figure 20 compare the capacity curves of the as-built and the upgraded structures with the results of the BNLDAs, expressed in terms of average maximum top displacement and maximum base shear force. The comparison confirms that Method A is more conservative than Method B, as already shown by NLSAs. In both directions and for both values of μ_{DB}, the average maximum displacement of Method B ($d_{p,B}$) is closer to the target displacement. In the Z-direction the values of $d_{p,B}$ are almost coincident with d_p with a maximum deviation of -4.3%, while the average maximum displacement of Method A ($d_{p,A}$) deviates by more than -15% (Table 3); in the X-direction the deviation is about -20% for Method B, while for Method A ranges from -20% to -32% depending on μ_{DB}. The introduction of dissipative braces produces an increase in the maximum base shear V_{max}, as shown in Figure 21. Consistently with the observed increase in PFA, Method A produces the largest increase on V_{max} (up to 41.5% more than in the as-built configuration), while Method B leads to a maximum increase of 20.5%.

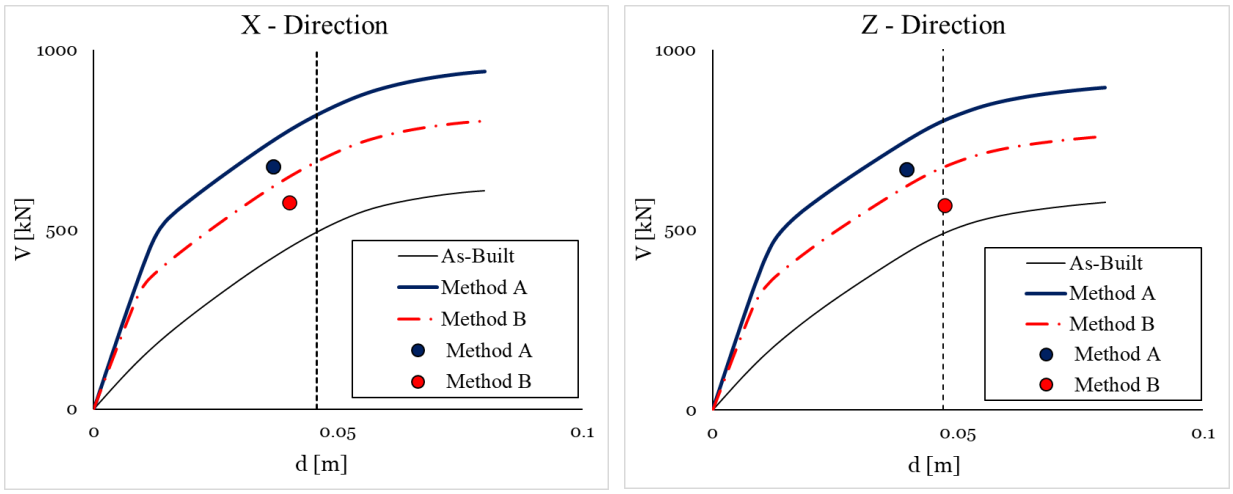

Figure 19: Comparison between capacity curves calculated by NLSA (solid lines) and maximum top displacement versus base shear force by BNLDA (dots), damped brace ductility $\mu_{DB} = 4$

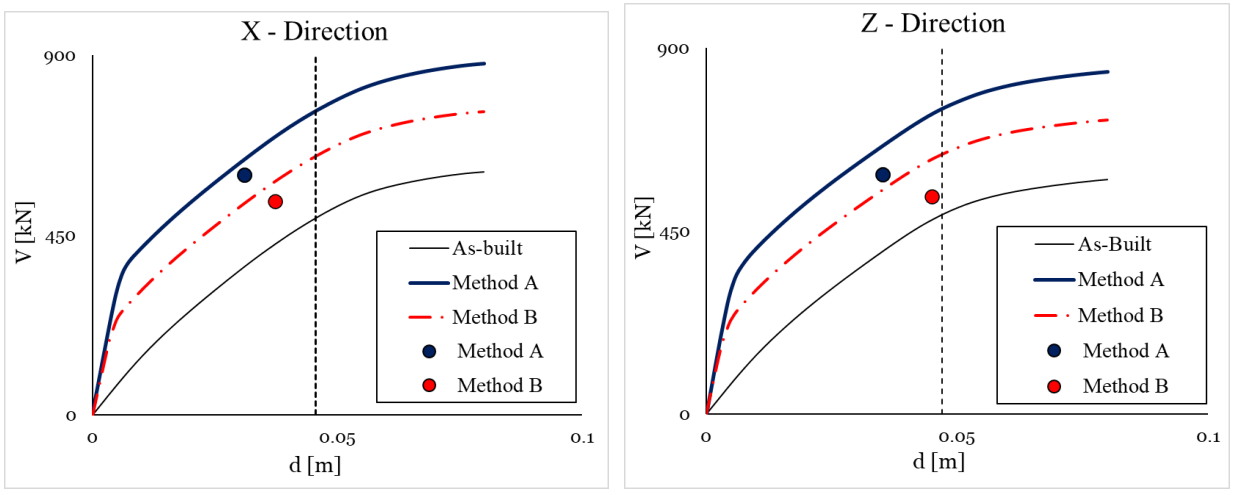

Figure 20: Comparison between capacity curves calculated by NLSA (solid lines) and maximum top displacement versus base shear force by BNLDA (dots), damped brace ductility $\mu_{DB} = 10$

	$\mu_{DB} = 4$					$\mu_{DB} = 10$			
Directions	d_p $[m]$	$d_{p,A}$ $[m]$	dev [%]	$d_{p,B}$ $[m]$	dev [%]	$d_{p,A}$ $[m]$	dev [%]	$d_{p,B}$ $[m]$	dev [%]
X	0.046	0.037	$\mathbf{-19.5}$	0.040	$\mathbf{-12.5}$	0.031	$\mathbf{-32}$	0.037	$\mathbf{-18.5}$

Z	0.047	0.040	**−15.6**	0.0473	**0.6**	0.035	**−25**	0.045	**−4.3**

Table 3: Comparison between the target displacement d_p and the average maximum top displacement of the damped braced frame with $\mu_{DB} = 4$ or $\mu_{DB} = 10$, and different distribution Method (A or B)

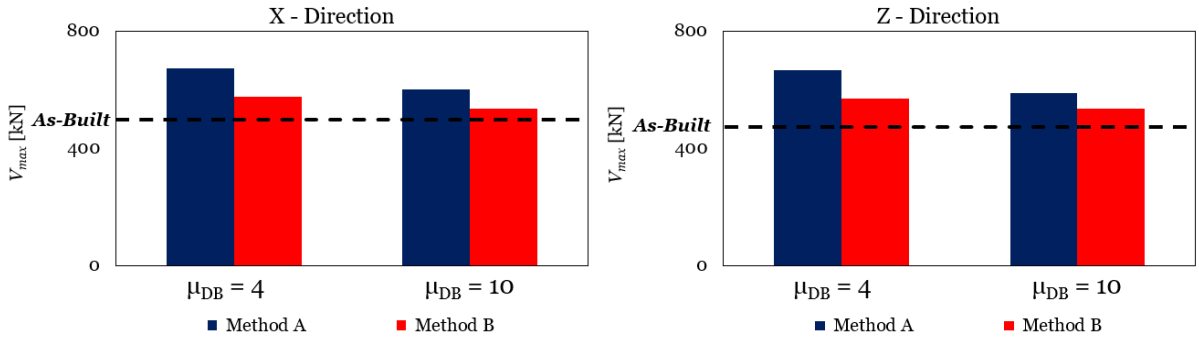

Figure 21: Comparison between the average maximum base shear force of the damped braced frame with $\mu_{DB} = 4$ or $\mu_{DB} = 10$, and different distribution Method (A or B); maximum base shear force of the as-built structure reported as broken line

In conclusion, the damped brace system designed according to proposed procedure in combination with the recommended distribution method (Method A) allows to fulfill the performance requirements for the upgraded frame. Alternative distribution methods, such as Method B, may look more effective by considering the global performance of the upgraded structure in terms of maximum top displacement and maximum base shear forces, as they provide floor drifts closer to the target performance without an excessive increase of the shear force at the base columns. However, as highlighted in Figure 15 and Figure 17, Method A provides a more effective control of the lateral deformation along the height of the building, ensuring that the maximum inter-story drift ratio is less than 0.5% at each floor, which is the goal of the retrofit design. In contrast, for Method B the target performance is found not satisfied at the second floor, whichever the assumed ductility factor. A further conclusion that is apparent from Figure 21 is that low-ductility damped braces turn out to be less effective for the control of both lateral drifts and shear forces of the main building.

3.3 Case-study 2: building in Pordenone

The second case-study is a residential 6-story building, designed in compliance with IBC [30] for a low seismicity zone corresponding to the municipality of Pordenone, Italy [45] (PGA = 1.91m/s^2, soil type B). This building is characterized by square 50x50cm columns at the ground level and at the first floor, and by square 40x40cm columns from the second to the last floor, Figure *9*. This arrangement results in a variation of stiffness along the height of the building and different floor masses at each story. The building is upgraded for a high seismicity area, considering the seismic loads provided by the code [30] for life-safety limit state (SLV), site of L'Aquila (Long 13° 23.9724', Lat 42° 21.033'), functional class cu = II, PGA = 4.062 m/s^2, soil type C and topographic factor T_2. Diagonal steel braces equipped with hysteretic devices are inserted in the facades, according to the layout shown in Figure *22* (4 units at each floor in both X and Z directions). In this case too, two ductility levels $\mu_{DB} = 4$ and $\mu_{DB} = 10$ are considered. Since the results are similar to those found for case-study 1, for brevity, only those relevant to the lateral deformation of the building are presented and discussed.

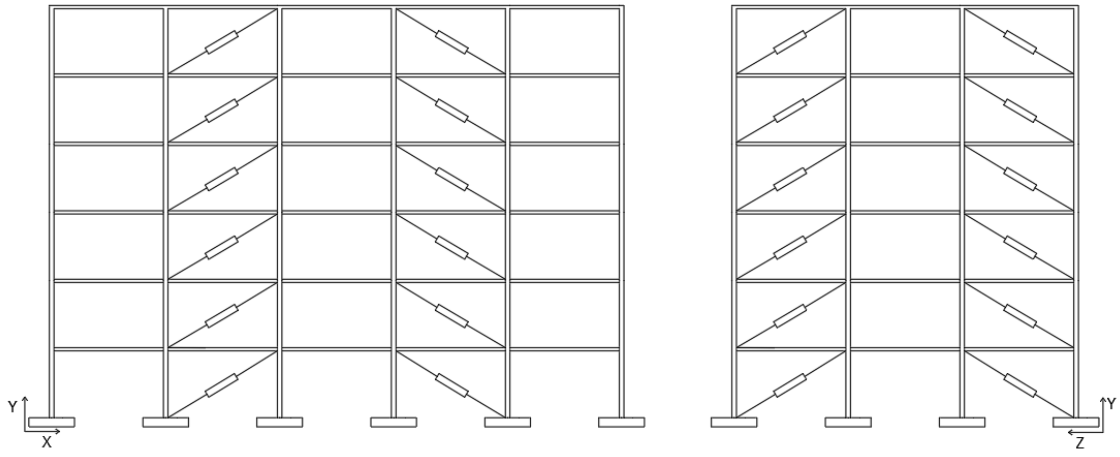

Figure 22: Diagonal layout of steel braces equipped with hysteretic dampers for case-study 2 building

As in case-study 1, the bilinear curve of the equivalent SDOF system of the as-built structure in either horizontal direction (X and Z) is determined from the MODAL capacity curve, Figure 23. The target

displacement is calculated considering a maximum inter-story drift of the braced structure equal to $\Delta_d = 0{,}005\ m/m$, to satisfy the stability requirement (STA) for non-structural elements at the ultimate limit state as recommended in [30]. Being h_0 = 3.0 m and $\delta_{i,max}$ = 0.2257, values of $d_p = 0.059\ m$ for the MDOF frame and d_p^* = 0.044 m for the equivalent SDOF system result. The parameters of the equivalent bilinear capacity curves of the main frame in the two horizontal directions are reported in Table 4Table *1*.

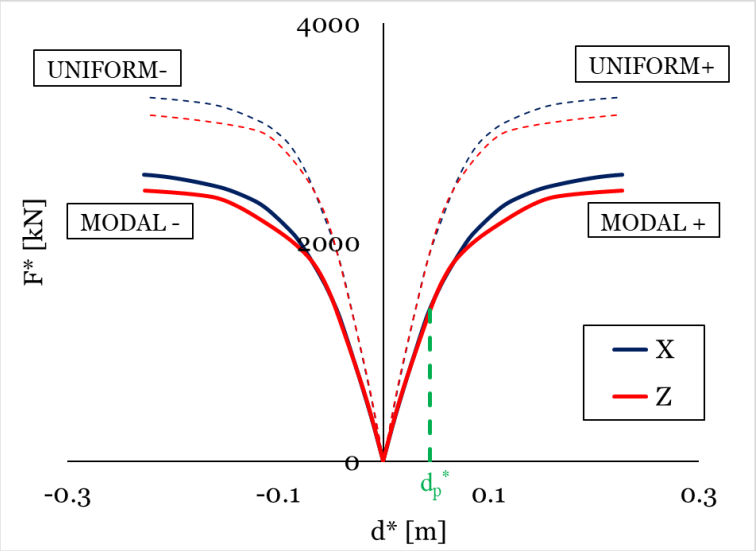

Figure 23: Capacity curves in X- and Z- direction

Direction	Γ $[-]$	d_y^* $[m]$	V_y^{*F} $[kN]$	d_p^* $[m]$	V_p^{*F} $[kN]$	ξ_F [%]	m^* $[ton]$
X	1.32	0.017	602.6	0.044	1387	2.2	958
Z	1.32	0.014	510	0.044	1368	2.4	956

Table 4: Properties of the equivalent SDOF system and bilinear capacity curves of case-study 2 structure in the two horizontal directions

The bilinear capacity curves in the X and Z directions are separately reported in the acceleration-displacement plane and the procedure described in Section 2.4 is iterated until the performance point

of the equivalent SDOF braced structure converges to the target displacement d_p^* with $\varepsilon \leq 0.05$. Figure 24 show the ADRS representation of the equivalent SDOF capacity curves along the X direction of the main frame (F) and the upgraded frame (F + DB). Convergence to values reported in Table 5 is obtained at the third iteration. It is to be noted that for the building under consideration, the properties of the equivalent SDOF damped brace along the two horizontal directions are practically the same.

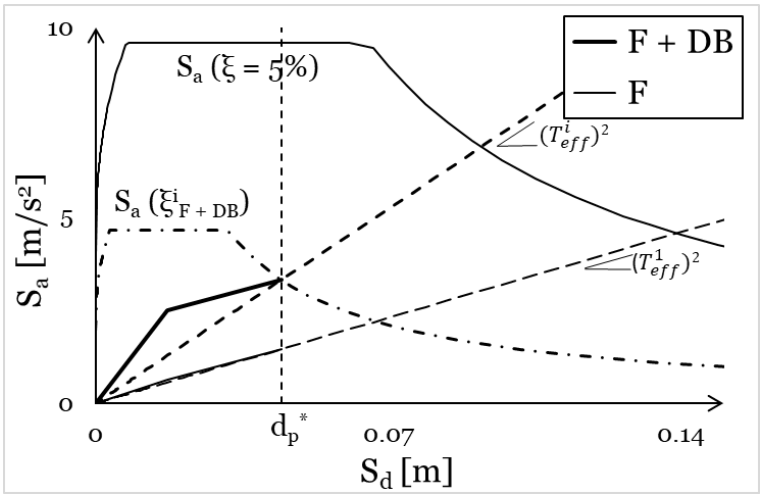

Figure 24: Equivalent capacity curves in X-direction of main Frame (F) and Frame + Damped brace (F + DB) with $\mu_{DB} = 10$

	X - Direction			Z - Direction		
$\boldsymbol{\mu_{DB}}$	V_y^{*DB} $[kN]$	d_p^* $[m]$	ξ_{DB} [%]	V_y^{*DB} $[kN]$	d_p^* $[m]$	ξ_{DB} [%]
4	2056	0.044	47.78	2045.5	0.044	47.78
10	1764.5	0.044	57.33	1756	0.044	57.33

Table 5: Properties of the SDOF damped brace for case-study 2

After the strength of the equivalent SDOF damped brace has been determined, the properties of the dissipative braces at each story are distributed in agreement with either Method A or Method B.

NLSAs are performed on both upgraded configurations and the relevant capacity curves are plotted in ADRS format to verify the effectiveness of the design, Figure 25. As expected, the distribution of stiffnesses and strengths according to Method A produces a stiffer global response.

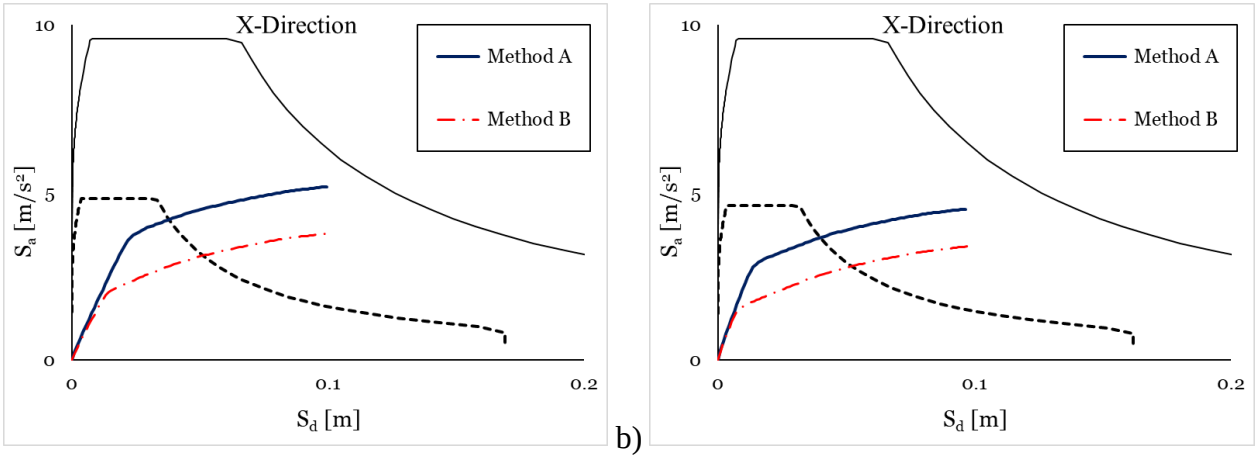

a) b)

Figure 25: Comparison of capacity curves in X-direction for damper brace ductility: a) $\mu_{DB} = 4$; b) $\mu_{DB} = 10$

BNLDAs are performed in conformity with IBC [30] and EC8 [47] considering two sets of seven artificial ground motions [67], compatible with the response spectrum defined by IBC [30].

Figure 26 and Figure *27* compare the capacity curves of the as-built and the upgraded structures with the results of the BNLDAs (average maximum top displacement and base shear force). Method B provides indeed an excellent agreement between structural displacement and the target value d_p^* for both ductility factors; with Method A the average BNLDA displacement coincides with the target value when the low ductility damper is considered, while for $\mu_{DB} = 10$ the method appears to be conservative, as already observed for case-1 building.

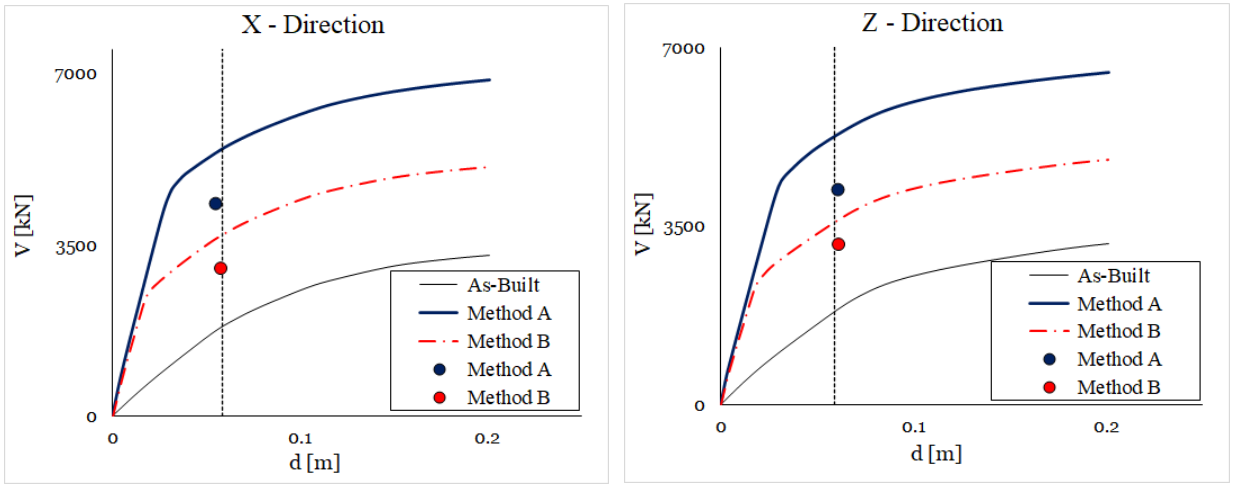

Figure 26: Comparison between capacity curves calculated by NLSA (solid lines) and maximum top displacement versus base shear force by BNLDA (dots), damped brace ductility $\mu_{DB} = 4$

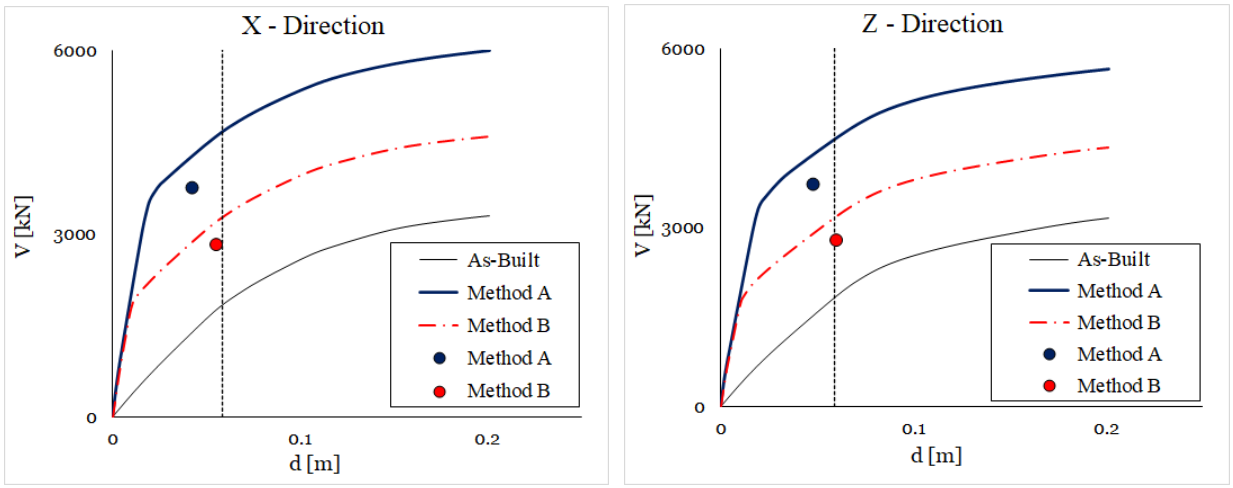

Figure 27: Comparison between capacity curves calculated by NLSA (solid lines) and maximum top displacement versus base shear force by BNLDA (dots), damped brace ductility $\mu_{DB} = 10$

However, the global response needs to be analyzed in conjunction with the local behavior. Figure 28 and Figure *29* show the maximum inter-story drift ratio Δ at each floor, comparing the as-built configuration with the upgraded configurations according to Method A and Method B.

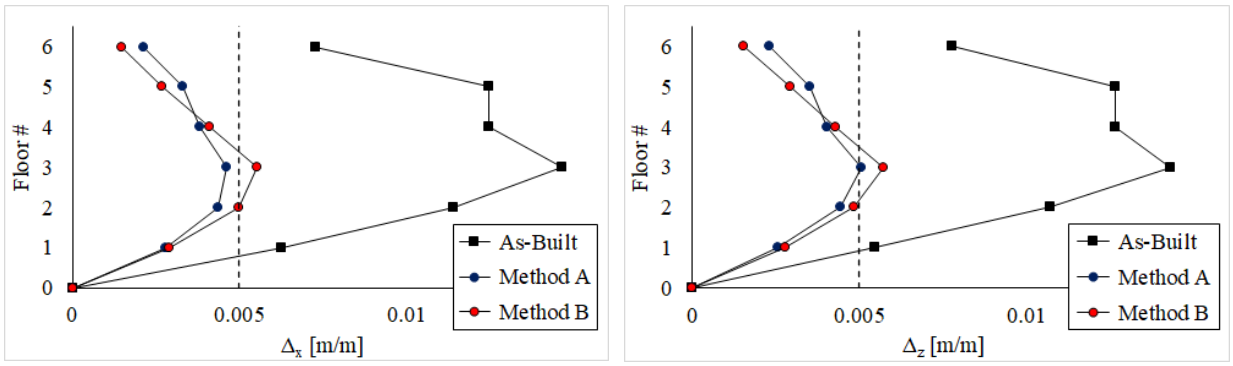

Figure 28: Maximum inter-story drift ratio Δ in X and Z directions obtained by BNLDAs with $\mu_{DB} = 4$

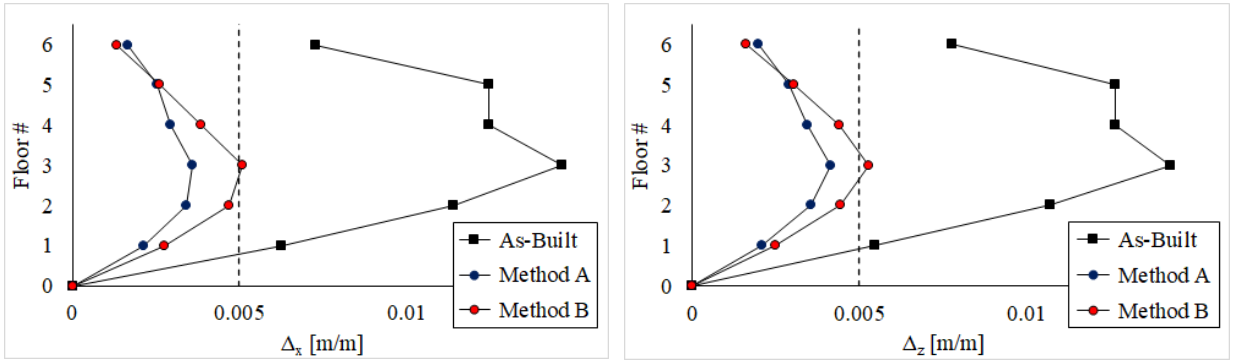

Figure 29: Maximum inter-story drift ratio Δ in X and Z directions obtained by BNLDAs with $\mu_{DB} = 10$

For $\mu_{DB} = 10$ (Figure *29*) the target drift ratio is substantially met at each floor with either damper distribution (only in Z direction, $\Delta = 0.0053$ m/m with Method B). In contrast, for $\mu_{DB} = 4$ (Figure *28*) only the distribution according to Method A meets the target, while with Method B at the third floor the drift ratio exceeds the limit in both X ($\Delta = 0.0055$ m/m) and Z ($\Delta = 0.0057$ m/m) directions.

4. Discussion and Conclusion

A displacement-based design procedure based on the Capacity Spectrum Method [46] has been developed for the seismic upgrade of frame structures via addition of hysteretic damped braces. A substitute structure consisting of an equivalent SDOF braced frame is introduced to represent the overall behavior of the existing frame and the damped brace system acting in parallel. The performance point for the upgraded structure is assigned in order to control the maximum inter-story drift, by assuming that the lateral deformation of the damped braced frame matches the first mode deformation of the main frame. The secant stiffness and the equivalent viscous damping ratio are used to characterize the non-linear behavior of the upgraded frame, which allows the direct calculation of the global properties of the hysteretic damper system.

The global stiffness and strength of the equivalent SDOF damped brace identified by the procedure are distributed along the height of the building according to a proportionality criterion which constrains the drifts of the braced frame to follow the first mode deformation of the main frame. The adopted distribution of the damped brace properties in elevation is expected to promote the simultaneous engagement of the dampers at each floor during the earthquake. Since the design methodology is based on the condensation of the MDOF structure to an equivalent SDOF system, the simultaneous engagement of the dampers along the height of the building is essential for the condensation to be accurate [13]. Moreover, ensuring that the first mode of the braced and unbraced frame is the same, it is also required for dimensioning the target displacement d_p according to Eqs. (5a) and (5b), which assume the proportionality of inter-story drifts of the upgraded and the main structure. Once the global stiffness and strength of the damped braces at each floor are determined, the properties of the single units are eventually calculated, depending on the selected brace configuration.

Even if some analogies exist with other approaches based on the response spectrum and utilizing either the initial stiffness ([18], [28]), or the secant stiffness to the maximum response level ([26],

[35]), the strength of the proposed method relies on its simplicity: only one NLSA of the as-built structure is performed at the beginning of the process, to determine the capacity curve of the main frame, and at each iteration the capacity curve of the upgraded frame is calculated by means of analytical equations accounting for the stiffness and the strength of the damped brace system. The iterative procedure can be implemented in a spreadsheet, and convergence is usually reached in few steps; in addition, the graphical representation of both curves in the ADRS plane has the added advantage of giving the engineer the opportunity to visualize at any iteration the relationship between demand and capacity.

Global approaches based on the definition of a capacity spectrum via an equivalent SDOF system have the merit to provide a simple, direct, and fast design procedure. However, as observed for similar approaches ([16]-[22], [28], [35], [53], [56]), in general they do not allow for a direct control of the drift demand at each floor To overcome this limit, a criterion based on the proportionality between the inter-story drift distribution of the upgraded and the modal properties of the main frame has been presented in the study. Though the distribution method is not intended to make the inter-story drift distribution more uniform, it allows to limit the lateral deformation of the weak story of the building to an assigned threshold associated to the design level of performance.

The effectiveness of the proposed distribution method (Method A) is assessed in comparison to a second method (Method B) which distributes the global properties based on a proportionality criterion with respect to floor stiffnesses calculated from NLSA ([28], [56]).

The two methods lead to differences in strengths and stiffnesses of the damped braces at each floor; this difference has a relatively low influence on the top displacement but has large effect on the distribution of the inter-story drifts. Namely, Method B was effective when dissipative braces with high ductility factor were considered, but it was unable to control the drift of the weak story of the frame when a damper with low ductility was selected. In contrast, the effectiveness of Method A was proved for both high and low μ_{DB} values. Another effect of the adopted distribution method regards

the increase in floor accelerations and in the internal forces of the structural elements of the main frame where the forces developed by the dampers are transferred (typically, the elements where the braces are connected). In this regard, the Method B examined in the case-studies seems to be more suitable, because of the lower strength and stiffness of the devices. However, in the proposed design method, the performance requirement is expressed in terms of target displacement and inter-story drift ratio, and in this respect the effectiveness of the recommended Method A is superior. Nevertheless, for different design requirements, e.g., when a main target is to control floor accelerations to protect acceleration-sensitive elements [31] or to limit the increase in axial load in weak elements, alternative distribution methods can be considered.

The presented procedure is directly applicable to low-rise and mid-rise buildings with in-plan and in-elevation regular distribution, for which the lateral deformation is essentially governed by the first mode, whereas it is not suitable for structures where the contribution of higher modes is not negligible. It should be noted that this does not represent a critical limitation from a practical point, given that in many countries, (e.g., Italy), the largest part of the existing building stock designed according to outdated codes, consists of low-rise and medium-rise buildings. Examples include residential buildings, schools, industrial sheds etc. [68]. The procedure, conceived for regular buildings, will be extended in a future study to in-elevation irregular frames and unsymmetric-plan structures.

Analogously, while only tested on RC structures in this study, the proposed procedure is applicable to steel structures as well. The extension of the approach to steel systems is the object of an ongoing investigation.

Owing to its ease, the procedure is aimed at enhancing the confidence of practitioners in using supplementary energy dissipation systems by providing a simple, fast, and handy procedure to tune the effective parameters of the damped braces. However, some limitations of the method exist, which are highlighted in the following points.

The case-studies have also highlighted that the global structural response estimated via BNLDAs is typically lower, in terms of base shear force and top displacement, than the one calculated via NLSAs of the MDOF braced frame system; this can be explained considering that the results of NLSAs depend on the considered lateral load distribution and in general neglect dynamic effects. Moreover, damped braces can provide an equivalent structural damping ξ_{F+DB} greater than 28% (as indeed occurred in the two case-studies examined in the study) which represents the limit over which the simplified shapes of pseudo-acceleration and displacement response spectra are no longer valid [29]. Therefore, the evaluation of $d = d_p$ carried out by referring to the displacement spectrum for $\xi = \xi_{F+DB}$ can provide only an approximate value of the displacement of the frame retrofitted with damped braces. These are inherent limits of all procedures for dimensioning of damped braces based on Direct-Displacement-Based Design (DDBD) method which exploit the capacity curves of the bare and retrofitted frame and the response demand spectra to evaluate the performance point.

The number and location of damping units to be installed in the structure, and their distribution along the height of the building, remain a design input which is to be decided by the user based on past experience or via trial and error. Evidently, the brace configuration cannot be standardized in a general procedure as it actually depends on specific constraints posed by e.g., architectural requirements, modification of the building layout, ability of structural members to resist the increased internal forces due to the braces and cost of strengthening procedures, etc.

The non-linear analyses presented in the study were performed considering artificial ground motions, because artificial accelerograms with smooth spectrum allow a more accurate control of the frame response than real accelerograms, usually characterized by a large scatter of spectral accelerations, thereby making the interpretation / comparison with NLSA simpler and more focused on the specific aspects that are analyzed in the work. In future developments the verification will be extended to include natural ground motions as well.

Symbols

b strain-hardening ratio

CR_1 curvature degradation parameter

CR_2 curvature degradation parameter

d_b diameter of longitudinal reinforcement

d_F roof displacement of the unbraced Multi Degree Of Freedom (MDOF) structure

d_F^* roof displacement of the unbraced Single Degree Of Freedom (SDOF) structure

d_D axial deflection of a hysteretic damper

d_e spectral displacement of an elastic oscillator with period T_{eff}

d_p target displacement of MDOF structure

$d_{p,A}$ averaged maximum displacement of damped braced frame according to distribution Method A

$d_{p,B}$ averaged maximum displacement of damped braced frame according to distribution Method B

d_p target displacement of MDOF structure

d_p^* target displacement of SDOF structure

d_u ultimate displacement of the unbraced MDOF structure

d_{uD} ultimate deflection of a hysteretic damper

d_u^{*DB} ultimate displacement of the equivalent SDOF damped brace

d_y yield displacement of the MDOF main structure

$d_{y,i}$ yield displacement of the i^{th} story of the main structure (with $i = 1 \div n$, where n is the total number of floors)

d_y^* yield displacement of the SDOF main structure

d_{yD} yield deflection of a hysteretic damper

d_y^{*DB} yield displacement of the equivalent SDOF damped brace

d_y^{*F} roof displacement at yielding of the unbraced SDOF structure

f_c compressive strength of concrete

F_i horizontal seismic force (with $i = 1 \div n$, where n is the total number of floors)

f_y yield stress of longitudinal steel reinforcement

F_{yi}^{DB} seismic lateral loads at yielding point of damped braces at the i^{th} floor (with $i = 1 \div n$, where n is the total number of floors)

h overall depth of beam or column

h_i inter-story height

h_0 uniform inter-story height

I_{eq} effective area moment of inertia of beam or column

I_g gross area moment of inertia of beam or column

K_D initial stiffness of the theoretical force–deflection curve of a hysteretic damper

$K_{2,D}$ post-yield stiffness of the theoretical force–deflection curve of a hysteretic damper

K_{eff} effective stiffness of the equivalent SDOF frame + damped brace system

K_F^* secant stiffness of the bilinear capacity curve to the target displacement

K_i^{DB} stiffness of the damped braces at the i^{th} story (with $i = 1 \div n$, where n is the total number of floors)

K_i^F stiffness of the i^{th} story of the as-built main structure (with $i = 1 \div n$, where n is the total number of floors)

L_{pl} plastic hinge length

m_i floor masses (with $i = 1 \div n$, where n is the total number of floors)

m^* equivalent mass of the SDOF structure

n_d total number of dampers per floor

N_D output force of a hysteretic damper

N_{yD} yield force of a hysteretic damper

N_{yi}^{DB} strength of the damped brace at the i^{th} story (with $i = 1 \div n$, where n is the total number of floors)

N_{uD} ultimate force of a hysteretic damper

PGA peak ground acceleration

PFA maximum peak floor acceleration across the frame

r hardening parameter of the theoretical force–deflection curve of a hysteretic damper

R_0 initial value of the curvature parameter

S_a acceleration spectrum

S_d displacement spectrum

T fundamental period

T_{eff} effective period of the equivalent SDOF frame + damped brace system

T_F^* effective period of the SDOF main structure

V_F base shear force of the MDOF main structure

V_F^* base shear force of the SDOF main structure

V_{max} averaged maximum base shear

V_p^{DB} ultimate strength of the MDOF damped brace

V_p^{*DB} ultimate strength of the SDOF damped brace

V_p^{*F} ultimate strength of the SDOF damped brace

V_y^{DB} yield strength of the MDOF damped brace

V_{yi}^{DB} yield shear force of damped brace at the i^{th} story (with $i = 1 \div n$, where n is the total number of floors)

V_y^{*DB} yield strength of the SDOF damped brace

V_y^F base shear force at yielding of the MDOF main structure

V_y^{*F} base shear force at yielding of the SDOF main structure

V_{yi}^F yield force of the i^{th} story of the main structure (with $i = 1 \div n$, where n is the total number of floors)

z distance from critical section of maximum curvature and the element point of contraflexure

Γ participation factor

δ_i difference between two consecutive first mode eigenvector components $= (\phi_i - \phi_{i-1})$

Δ_d target inter-story drift ratio

Δ_i maximum inter-story drift ratio at the i^{th} story

ξ structural viscous damping ratio

ξ_{DB} equivalent viscous damping ratio of the damped brace system

ξ_{eff} required equivalent viscous damping ratio

ξ_F equivalent viscous damping ratio of the main structure (unbraced)

ξ_{F+DB} equivalent viscous damping ratio of the equivalent SDOF frame + damped brace

κ_{DB} coefficient accounting for the energy dissipation capacity of the damped brace

κ_F coefficient accounting for the energy dissipation capacity of the main structure

μ_{DB} ductility of the damped brace

μ_F ductility of the main structure

ϕ_i first mode eigenvector component (with $i = 1 \div n$, where n is the total number of floors)

Acknowledgments

This work was funded by the Italian Department of Civil Protection (DPC) in the frame of the national Research Project DPC-ReLUIS 2019–2021 Work Package WP 15 "Contributi normativi a isolamento e dissipazione".

The work was developed during the research fellowship of Eleonora Bruschi at the University of Washington sponsored by the Ermenegildo Zegna Founder's Scholarship (2018).

References

[1] Christopolous C, Filiatrault A. Principles of passive supplemental damping and seismic isolation. IUSS Press 2006, Pavia.

[2] Kim J, Choi H. Displacement-Based Design of supplemental dampers for seismic retrofit of a framed structure, Journal of Structural Engineering 2006; 132(6): 873-883; DOI:10.1061.

[3] Ferraioli M, Lavino A. A Displacement-Based Design Method for seismic retrofit of RC buildings using dissipative braces, Hindawi, Mathematical Problems in Engineering 2018; Volume 2018, Article ID 5364564, 28 pages; DOI: 10.1155/2018/5364564.

[4] Priestley MJN. Myths and fallacies in earthquake engineering-conflicts between design and reality, Bulletin of New Zealand Society for Earthquake Engineering 1993; 26(3): 329-341; DOI: 10.5459/bnzsee.26.3.329-341.

[5] Noruzvand M, Mohebbi M, Shakeri K. Modified direct displacement-based design approach for structures equipped with fluid viscous damper, Structural Control and Health Monitoring 2020; 27: e2465; DOI: 10.1002/stc.2465.

[6] Lin YY, Tsai MH, Hwang JS, Chang KC. Direct Displacement-Based Design for buildings with passive energy dissipation systems, Engineering Structures 2003; 25(1): 25-37; DOI: 10.1016/S0141-0296(02)00099-8.

[7] Pennuci D, Calvi GM, Sullivan TJ. Displacement-Based Design of precast walls with additional dampers, Journal of Earthquake Engineering 2009; 13(1): 40–65; DOI: 10.1080/13632460902813265.

[8] Wijesundara KK, Nascimbene R, Sullivan TJ. Equivalent viscous damping for steel concentrically braced frame structures, Bulletin of Earthquake Engineering 2011; (9): 1535-1558; DOI 10.1007/s10518-011-9272-4.

[9] Sullivan TJ, Lago A. Towards a simplified Direct DBD procedure for the seismic design of moment resisting frames with viscous dampers, Engineering Structures 2012; (35): 140-148; DOI: 10.1016/j.engstruct.2011.11.010.

[10] O'Reilly GJ, Sullivan TJ. Direct Displacement-Based seismic design of eccentrically braced steel frames, Journal of Earthquake Engineering 2016; 20(2): 243-278; DOI: 10.1080/13632469.2015.1061465.

[11] Segovia VA, Ruiz SE. Direct Displacement-Based Design for buildings with hysteretic dampers, using best combinations of stiffness and strength ratios; Journal of Earthquake Engineering 2017; 21(5): 752-775; DOI: 10.1080/13632469.2016.1185054.

[12] Sahoo DR, Prakash A. Seismic behavior of concentrically braced frames designed using direct displacement-based method, International Journal of Steel Structures 2019; 19(1): 96-109; DOI: 10.1007/s13296-018-0092-0.

[13] Levy R, Lavan O, Rutenberg A. Seismic Design of Friction Damped Braced Frames Based on Historical Records, Earthquake Spectra 2005; 21(3): 761-778.

[14] Seismology (1999). Recommended Lateral Force Requirements and Commentary, Seismology Committee, Structural Engineers Association of California, SEAOC.

[15] ATC (1996) Seismic evaluation and retrofit of concrete buildings. ATC-40, Applied Technology Council, Redwood City, California.

[16] Mazza F, Vulcano A. Displacement-Based Seismic Design procedure for framed buildings with dissipative braces Part I: Theoretical formulation, Seismic Engineering Conference Commemorating the 1908 Messina and Reggio Calabria Earthquake (MERCEA08), Reggio Calabria, Italy. American Institute of Physics Conference Proceedings 2008a, U.S.A, Vol. 1020 (part two), 1399-1406.

[17] Mazza F, Vulcano A. Displacement-Based Seismic Design procedure for framed buildings with dissipative braces Part II: Numerical Results, Seismic Engineering Conference Commemorating the 1908 Messina and Reggio Calabria Earthquake (MERCEA08), Reggio Calabria, Italy. American Institute of Physics Conference Proceedings 2008b, U.S.A, Vol. 1020 (part two), 1407-1416.

[18] Mazza F, Vulcano A. Displacement-Based Design procedure of damped braces for the seismic retrofitting of RC framed buildings, Bulletin of Earthquake Engineering 2015; (13): 2121-2143; DOI: 10.1007/s10518-014-9709-7.

[19] Mazza F, Vulcano A. Displacement-Based seismic Design of hysteretic damped braces for retrofitting in-elevation irregular RC framed buildings, Soil Dynamics and Earthquake Engineering 2015; 69: 115-124; DOI: 10.1016/j.soildyn.2014.10.029.

[20] Mazza F, Vulcano A. Nonlinear seismic analysis of r.c. framed buildings with setbacks retrofitted by damped braces, Engineering Structures 2016; 126: 559-570; DOI: 10.1016/j.engstruct.2016.07.055.

[21] Mazza F. Nonlinear seismic analysis of unsymmetric-plan structures retrofitted by hysteretic damped braces, Bulletin of Earthquake Engineering 2016; 14: 1311-1331; DOI: 10.1007/s10518-016-9873-z.

[22] Mazza F, Pedace E, Del Favero F. Effectiveness of damped braces to mitigate seismic torsional response of unsymmetric-plan buildings, Mechanical Systems and Signal Processing 2017; 85: 610-624; DOI: 10.1016/j.ymssp.2016.09.003.

[23] Lin YY, Chang KC, Chen CY. Direct Displacement-Based Design for seismic retrofit of existing buildings using nonlinear viscous dampers, Bulletin of Earthquake Engineering 2008; 6: 535-552; DOI 10.1007/s10518-008-9062-9.

[24] Londono JM, Wagg DJ, Neild SA. Supporting brace sizing in structures with added linear viscous fluid dampers: A filter design solution, Earthquake Engineering & Structural Dynamics 2014; 43: 1999-2013; DOI: 10.1002/eqe.

[25] Raju KR, Ansu M, Iyer NR. A methodology of design for seismic performance enhancement of buildings using viscous fluid dampers, Structural Control and Health Monitoring 2014; 21: 342-355; DOI: 10.1002/stc.1568.

[26] Bergami AV, Nuti C. A design procedure of dissipative braces for seismic upgrading structures, Earthquakes and Structures 2013; 4(1): 85-105; DOI: 10.12989/eas.2013.4.1.085.

[27] Fajfar P. Capacity spectrum method based on inelastic demand spectra, Earthquake Engineering & Structural Dynamics 1999; 28(9): 979-993.

[28] Di Cesare A, Ponzo FC. Seismic retrofit of reinforced concrete frame buildings with hysteretic bracing systems: design procedure and behaviour factor, Hindawi, Shock and Vibration 2017; Volume 2017, Article ID 2639361; DOI: 10.1155/2017/2639361.

[29] CEN (European Committee for Standardization). Design of structures for earthquake resistance - Part 3: Assessment and retrofitting of buildings. EN 1998–3 Eurocode 8; 2005.

[30] CSLLPP (Consiglio Superiore dei Lavori Pubblici). D.M. 17 gennaio 2018 in materia di "norme tecniche per le costruzioni". Gazzetta ufficiale n.42 del 20 febbraio 2018, Supplemento ordinario n.8, Ministero delle Infrastrutture e dei trasporti, Roma; 2018, in Italian.

[31] Gandelli E, Taras A, Disti J, Quaglini V. Seismic retrofit of hospitals by means of hysteretic braces: influence on acceleration-sensitive non-structural components. Frontiers in Built Environment 2019; 5(100); DOI: doi.org/10.3389/fbuil.2019.00100.

[32] Carofilis W, Perrone D, O'Reilly GJ, Monteiro R, Filiatrault A. Seismic retrofit of existing school buildings in Italy: Performance evaluation and loss estimation, Engineering Structures 2020; 225; DOI: 10.1016/j.engstruct.2020.111243.

[33] Barbagallo F, Bosco M, Marino EM, Rossi PP, Stramondo P. A multi-performance design method for seismic upgrading of existing RC frames by BRBs, Earthquake Engineering & Structural Dynamics 2017; 46: 1099-1119; DOI: 10.1002/eqe.

[34] Antoniou S, Pinho R. Development and verification of a displacement-based adaptive pushover procedure, Journal of Earthquake Engineering 2004; (8)5: 643-661; DOI: 10.1080/13632460409350504.

[35] Nuzzo I, Losanno D, Caterino N. Seismic design and retrofit of frames structures with hysteretic dampers: a simplified displacement-based procedure, Bulletin of Earthquake Engineering 2019; 17: 2787-2819; DOI: 10.1007/s10518-019-00558-8.

[36] Nuzzo I, Losanno D, Caterino N. DIBRAST: A computer-aided seismic design procedure for frame structures equipped with hysteretic devices, Frontiers in Built Environment 2020; 6(13); DOI: 10.3389/fbuil.2020.00013.

[37] Diotallevi PP, Landi L, Dellavalle A. A methodology for the direct assessment of the damping ratio of structures equipped with nonlinear viscous dampers, Journal of Earthquake Engineering 2012; 16(3): 350-373; DOI: 10.1080/13632469.2011.618521.

[38] Landi L, Fabbri O, Diotallevi PP. A two-step direct method for estimating the seismic response of nonlinear structures equipped with nonlinear viscous dampers, Earthquake Engineering & Structural Dynamics 2014; 43(11): 1641-1659; DOI: 10.1002/eq.

[39] Silvestri S, Gasparini G, Trombetti T. A five-step procedure for the dimensioning of viscous dampers to be inserted in building structures, Journal of Earthquake Engineering 2010; 14(3): 417-447; DOI: 10.1080/13632460903093891.

[40] Palermo M, Muscio S, Silvestri S, Landi L, Trombetti T. On the dimensioning of viscous dampers for the mitigation of the earthquake-induced effects in moment-resisting frame structures, Bulletin of Earthquake Engineering 2013; 11(6): 2429-2446.

[41] Durucan C, Dicleli M. Analytical study on seismic retroftting of reinforced concrete buildings using steel braces with shear link. Engineering Structures 2010; 32(10): 2995-3010; DOI: 10.1016/j.engstruct.2010.05.019.

[42] Terenzi G. Energy-Based Design criterion of dissipative bracing systems for the seismic retrofit of frame structures, Applied Science 2018; 8(2), 268; DOI :10.3390.

[43] Sorace S, Terenzi G. Seismic protection of framed structures by fluid viscous damped braces, Journal of Structural Engineering 2008; 134(1): 45-55; DOI: 10.1061/(ASCE)0733-9445(2008)134:1(45).

[44] De Domenico D, Ricciardi G, Takewaki I. Design strategies of viscous dampers for seismic protection of building structures: A review, Soil Dynamics and Earthquake Engineering 2019; 118: 144-165; DOI: 10.1016/j.soildyn.2018.12.024.

[45] Faleschini F, Zanini MA, Toska K. Seismic reliability assessment of code-conforming reinforced concrete buildings made with electric arc furnace slag aggregates, Engineering Structures 2019; 195: 324-339; DOI: 10.1016/j.engstruct.2019.05.083.

[46] Freeman SA. The Capacity Spectrum Method as a tool for seismic design, Proceedings of the 11th European Conference on Earthquake Engineering 1998, Sept 6-11, Paris.

[47] CEN (European Committee for Standardization). Design of structures for earthquake resistance - Part 1: General rules, seismic actions and rules for building. EN 1998–1 Eurocode 8; 2005.

[48] Quaglini V, Pettorruso C, Bruschi E. Experimental and numerical assessment of prestressed lead extrusion dampers, International Journal of Earthquake Engineering 2021; 2.

[49] Dwairi HM, Kowalsky MJ, Nau JM. Equivalent damping in support of Direct Displacement-Based Design, Journal of Earthquake Engineering 2007; 11(4): 512-530; DOI: 10.1080/13632460601033884.

[50] CSLLPP (Consiglio Superiore dei Lavori Pubblici). Circolare 21 gennaio 2019, n. 7 C.S.LL.PP. Istruzioni per l'applicazione dell'«Aggiornamento delle "Norme tecniche per le costruzioni"» di cui al decreto ministeriale 17 gennaio 2018, Roma; 2019, in Italian.

[51] Sousa R, Almeida JP, Correia AA, Pinho R. Shake table blind prediction tests: Contributions for improved fiber-based frame modelling, Journal of Earthquake Engineering 2020; 24(9): 1435-1476; DOI: 10.1080/13632469.2018.1466743.

[52] Correira AA, Almeida JP, Pinho R. Seismic energy dissipation in inelastic frames: Understanding state-of-the-practice damping models, Structural Engineering International 2013; 23(2): 148-158; DOI: 10.2749/101686613X13439149157001.

[53] Mazza F, Vulcano A. Design of hysteretic damped braces to improve the seismic performance of steel and R.C. framed structures, International Journal of Earthquake Engineering 2014; 31(1): 5-16.

[54] Kudu FN, Uçak S, Osmancikli G, Türker T, Bayraktar A. Estimation of damping ratios of steel structures by Operational Modal Analysis Method, Journal of Constructional Steel Research 2015; 112: 61-68; DOI: 10.1016/j.jcsr.2015.04.019.

[55] Mahaney JA, Paret TF, Kehoe BE, Freeman SA. The Capacity Spectrum Method for evaluating structural response during the Loma Prieta earthquake, 1993 National Earthquake Conference, Memphis, TN.

[56] Ponzo FC, Di Cesare A, Arleo G, Totaro P. Protezione sismica di edifici esistenti con controventi dissipativi di tipo isteretico: aspetti progettuali ed esecutivi, Progettazione Sismica 2010; II(1): 19-42.

[57] Martinez-Rueda JE. On the evolution of energy dissipation devices for seismic design, Earthquake Spectra 2002; 18(2): 309-346.

[58] McKenna F, Fenves GI, Scott MH. Open System for Earthquake Engineering Simulation, PEER Report, Berkeley, CA; 2000.

[59] Scott MH, Fenves GL. Plastic Hinge Integration Methods for Force-Based Beam-Column Elements, Journal of Structural Engineering 2006; 132(2): 244-252; DOI: 10.1061/(ASCE)0733-9445(2006)132:2(244).

[60] OpenSeesWiki online manual. Available online at: https://opensees.berkeley.edu/wiki/index.php/Main_Page [last access: April 2021].

[61] Bruschi E, Calvi PM, Quaglini V. Concentrated plasticity modelling of RC frames in time-history analyses, Engineering Structures 2021; 243: 112716; DOI: 10.1016/j.engstruct.2021.112716.

[62] Menegotto M, Pinto PE. Method of analysis for cyclically loaded RC plane frames including changes in geometry and non-elastic behaviour of elements under combined normal force and bending, IABSE: Symposium on resistance and ultimate deformability of structures acted on by well defined repeated loads 1973 – Final Report.

[63] Filippou FC, Popov EP, Bertero VV. Effects of Bond Deterioration on Hysteretic Behavior of Reinforced Concrete Joints, Report EERC 83-19 (1983), Earthquake Engineering Research Center, University of California, Berkeley.

[64] Popovics S. A numerical approach to the complete stress-strain curve of concrete, Cement and Concrete Research 1973; 3(5): 583-599.

[65] Barbagallo F, Bosco M, Marino E, Rossi P. On the fibre modelling of beams in RC framed buildings with rigid diaphragm, Bulletin of Earthquake Engineering 2020; 18: 189-210; DOI: 10.1007/s10518-019-00723-z.

[66] Mazzoni S, McKenna F, Scott MH, Fenves GL, Jeremic B. OpenSEES command language manual. Pacific Earthquake Engineering Research Center, University of California, Berkeley, 2003.

[67] SIMQKE (SIMulation of earthQuaKE ground motions). Available online at: https://gelfi.unibs.it/software/simqke/simqke_gr.htm (last accessed: July 2021).

[68] CRESME Ricerche, Incentivi e riduzione del rischio sismico in Italia, Ingegneria Sismica Italiana, 2020, in Italian.